Supporting information

Efficient SF_6 capture and separation in robust gallium- and vanadium metal-organic frameworks

Michelle Åhlén,[a] Yi Zhou,*[b,c] Daniel Hedbom,[a] Hae Sung Cho,[b,c,d] Maria Strømme,[a] Osamu Terasaki,[b,c] Ocean Cheung*[a]

[a]Division of Nanotechnology and Functional Materials, Department of Materials Science and Engineering, Uppsala University, Ångström Laboratory, Uppsala SE-751 03, Box 35, Sweden.

[b]Centre for High-resolution Electron Microscopy (Cℏ EM), School of Physical Science and Technology, ShanghaiTech University, Shanghai, 201210, People's Republic of China.

[c]Shanghai Key Laboratory of High-resolution Electron Microscopy, ShanghaiTech University, Shanghai, 201210, People's Republic of China

[d]Department of Chemistry, Chung-Ang University, 06974 Seoul, Republic of Korea

Corresponding authors: yizhou@whu.edu.cn; ocean.cheung@angstrom.uu.se

Table of contents

Section S1. Materials and methods

Materials

N,N-dimethylformamide (DMF), and Acetic acid ≥99% were purchased from VWR International AB, Sweden. Vanadyl(IV) sulfate hydrate ($VOSO_4 \cdot xH_2O$), Gallium(III) nitrate hydrate ($Ga(NO_3)_3 \cdot xH_2O$), 1,3,6,8-tetrakis(4-carboxyphenyl)pyrene (H_4TBAPy), and 1,2,4,5-tetrakis(4-carboxyphenyl)benzene (H_4TCPB) were purchased from Sigma-Aldrich, USA. All chemicals were used as received without further purification.

Preparation of V-TBAPy and -TCPB

In a typical procedure, $VOSO_4 \cdot xH_2O$ (0.20 mmol) and H_4TBAPy (0.20 mmol) were dispersed in 10 ml DMF. The yellow dispersion was thereafter transferred to a 25 ml Teflon—lined stainless steel autoclave and heated at 180 ˚C for 72 h. The obtained green product was collected by centrifugation at 3,800 rpm for 20 min, washed once with deionized water and twice with DMF, and finally dried overnight in a ventilated oven at 70 ˚C. V-TCPB was synthesized in the same manner using H_4TCPB (0.20 mmol) as the organic linker instead.

Preparation of Ga-TBAPy and -TCPB

Ga-TBAPy was prepared from a solvothermal synthesis of $Ga(NO_3)_3 \cdot xH_2O$ (0.167 mmol) and H_4TBAPy (0.167 mmol) in a mixture of 11.5 mL DMF and 1.0 mL acetic acid at 120 °C for 48 h in a Teflon-lined stainless steel autoclave. The product was collected by centrifugation at 3,800 rpm for 20 min, washed with DMF three times, and finally dried overnight in a ventilated oven at 70 °C. Similarly, Ga-TCPB was synthesized according to the same procedure using H_4TCPB as the linker.

Characterization

Powder X-ray diffraction (PXRD) diffractograms were recorded on a Bruker D8 Advanced Powder diffractometer (Bruker, Bremen, Germany) operated at 40 kV and 40 mA, using Cu Kα radiation (λ = 1.5418 Å), a step-size of 0.02 ˚ and a time-per-step of 0.5 s. Scanning electron microscopy (SEM) images were obtained on a Zeiss Merlin Field Emission Scanning Electron Microscope (Oberkochen, Germany) using an acceleration voltage of 2.5 kV and a probe current of 80 pA. All samples were sputter-coated with a thin layer of Pd/Au prior to imaging.

Section S2. Structure determination

The structures of the Ga- and V-based MOFs were determined using 3-dimensional electron diffraction (3D ED) combined with high-resolution transmission electron microscopy (HRTEM) imaging, as well as structure modeling. The samples were dispersed in absolute ethanol and a droplet of the suspensions was transferred onto carbon-coated copper grids. The 3D ED data sets were collected on a JEOL JEM-F200 TEM (Tokyo, Japan) operated at an accelerating voltage of 200 kV using an ASI Cheetah 1800 detector under continuous tilting mode. The data was analyzed and visualized using the software *EDT PROCESS* [1] for the determination of unit-cell parameters and reflection conditions and processed by the X-ray Detector Software *XDS* [2] for extraction of reflection intensities which were subsequently used for structure solution. Using *Olex2* [3], the structure was solved with the integrated space-group and crystal-structure determination program *SHELXT* [4] using Intrinsic Phasing and refined with the *SHELXL* [5] refinement package using Least Squares minimization. Selected area electron diffraction (SAED) and HRTEM images were obtained on a JEOL JEM-2100Plus TEM (Tokyo, Japan) using a TVIPS XF416 detector.

Le Bail and Rietveld refinements [6, 7] of the MOFs were performed using the crystallographic program *JANA* [8] over the full sampled angular range based on space group *P2/m* for V- and Ga-TBAPy, Ga-TCPB, and *Pcma* for V-TCPB. The Bragg peaks were modeled by a Pseudo-Voigt peak-shape function modified for asymmetry, with six coefficients that could be refined. The background was treated using a Legendre polynomial with six parameters that could be refined for the samples. The starting atomic coordinates were adopted from the model obtained by 3D ED data. Because of the complexity of the structural model, constraints on V-O, Ga-O, C-O, and C-C distances were applied, and their weight was removed in the final cycles. All materials were visualized by using the 3D visualization program *VESTA* [9].

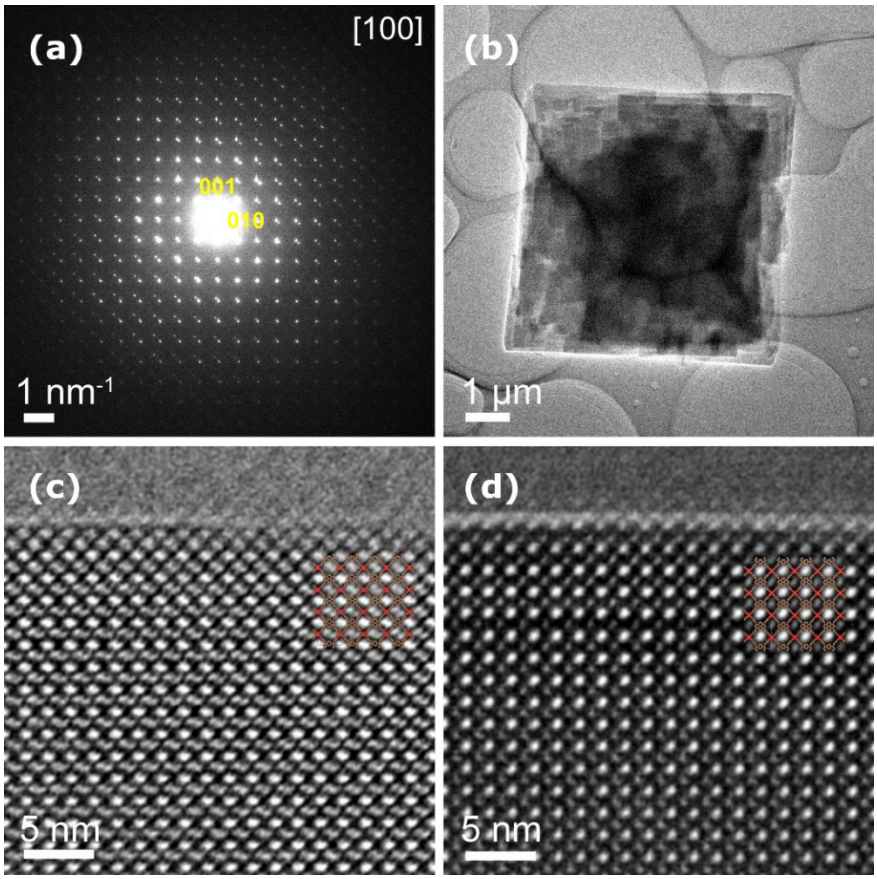

Fig. S1. (a) Selected area electron diffraction pattern, (b) low magnification bright-field image, and (c – d) corresponding high-resolution TEM images of V-TBAPy with an insert of the structure model.

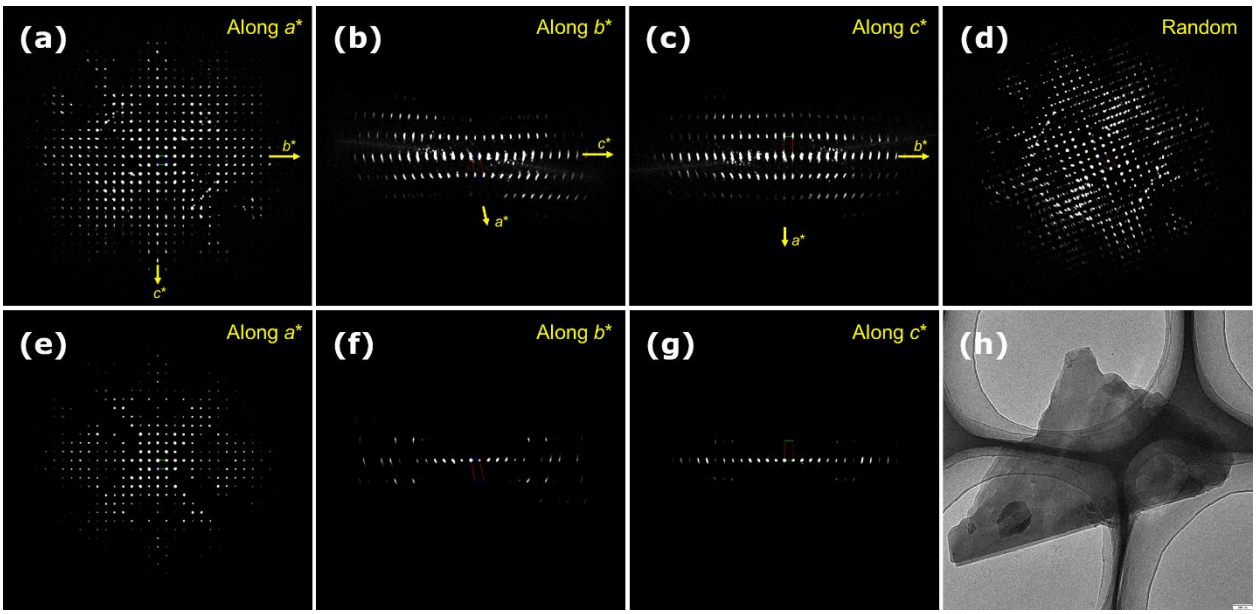

Fig. S2. (a – d) projection view of the 3D reciprocal lattice of V-TBAPy, (e – g) 2D slices from the reconstructed 3D reciprocal lattice as obtained from the 3D ED data, and (h) low magnification bright-field image of the crystal.

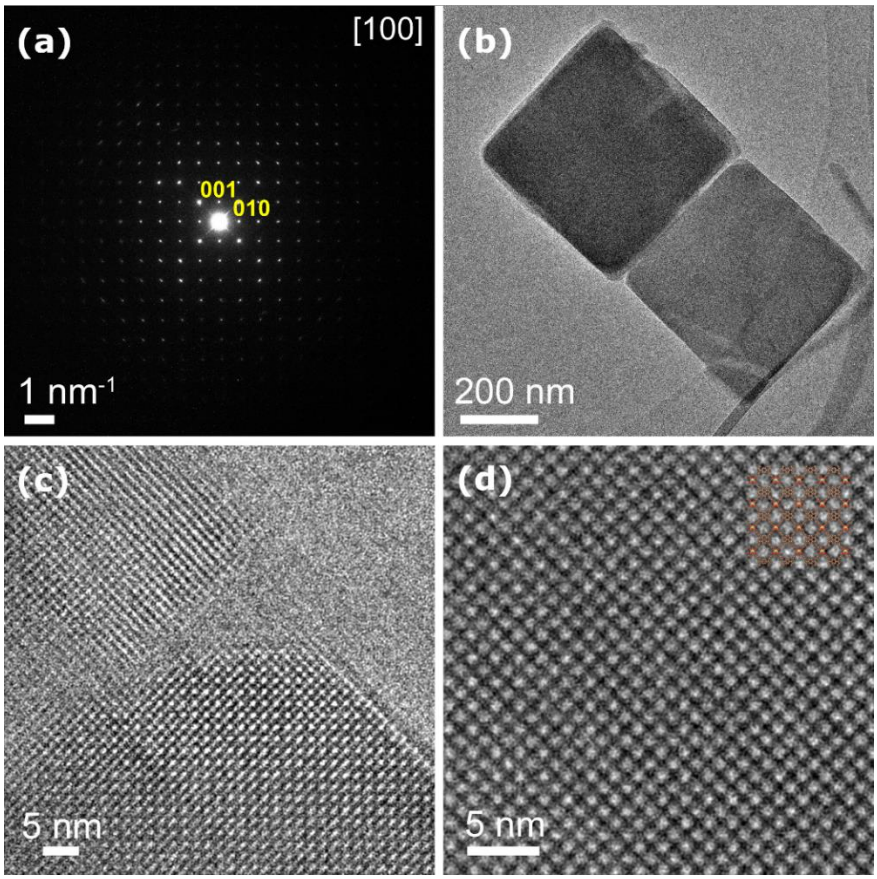

Fig. S3. (a) Selected area electron diffraction pattern, (b) low magnification bright-field image, and (c – d) corresponding high-resolution TEM images of Ga-TBAPy with an insert of the structure model.

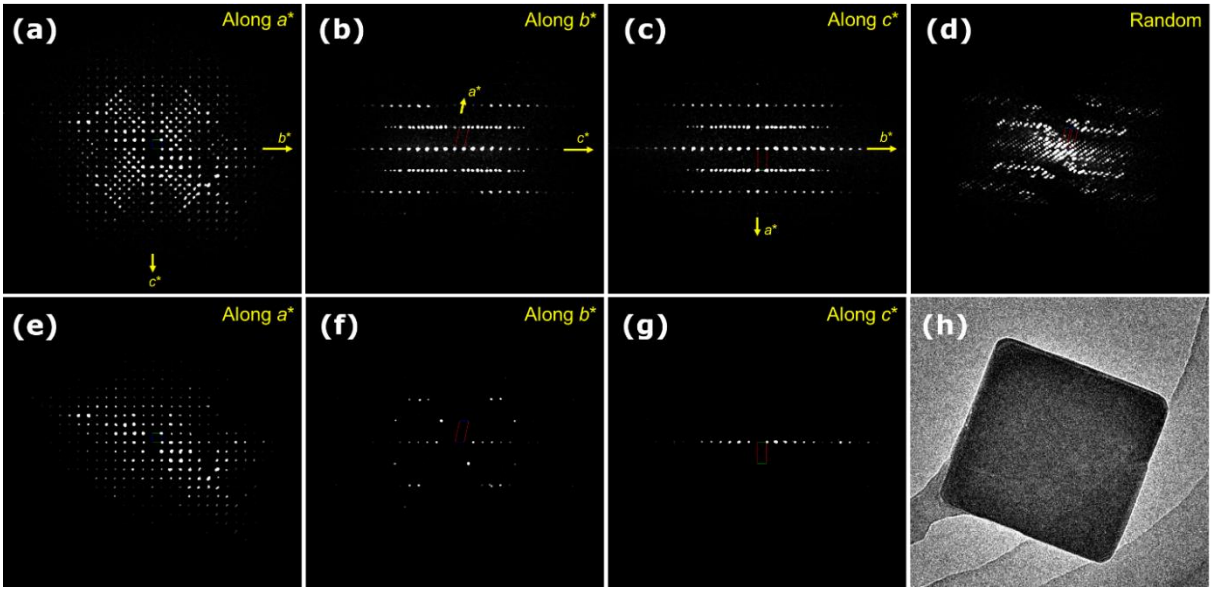

Fig. S4. (a – d) projection view of the 3D reciprocal lattice of Ga-TBAPy, (e – g) 2D slices from the reconstructed 3D reciprocal lattice as obtained from the 3D ED data, and (h) low magnification bright-field image of the crystal.

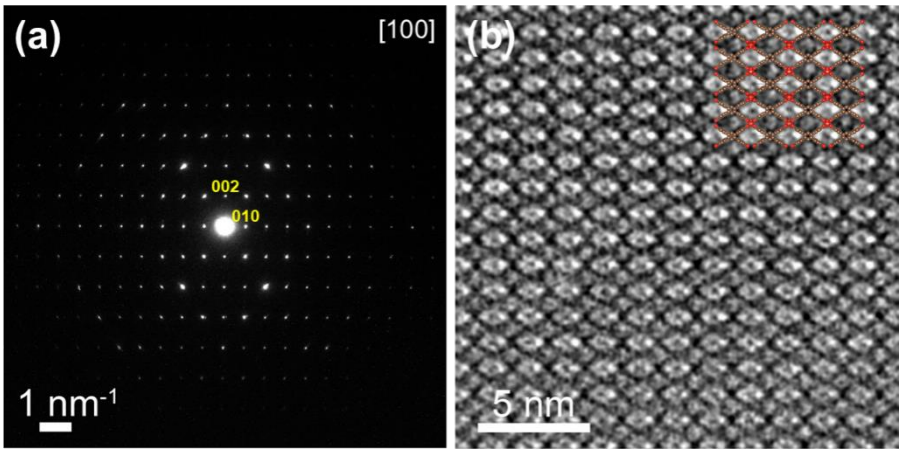

Fig. S5. (a) Selected area electron diffraction pattern and (b) the corresponding high-resolution TEM image of V-TCPB with an insert of the structure model.

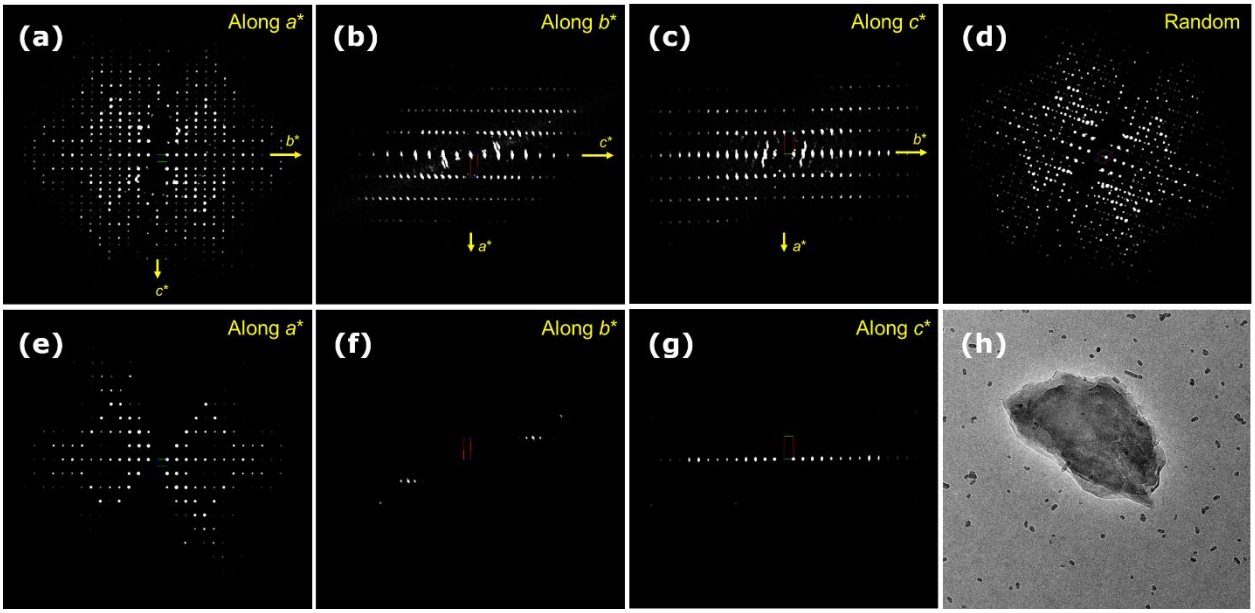

Fig. S6. (a – d) projection view of the 3D reciprocal lattice of V-TCPB, (e – g) 2D slices from the reconstructed 3D reciprocal lattice as obtained from the 3D ED data, and (h) low magnification bright-field image of the crystal.

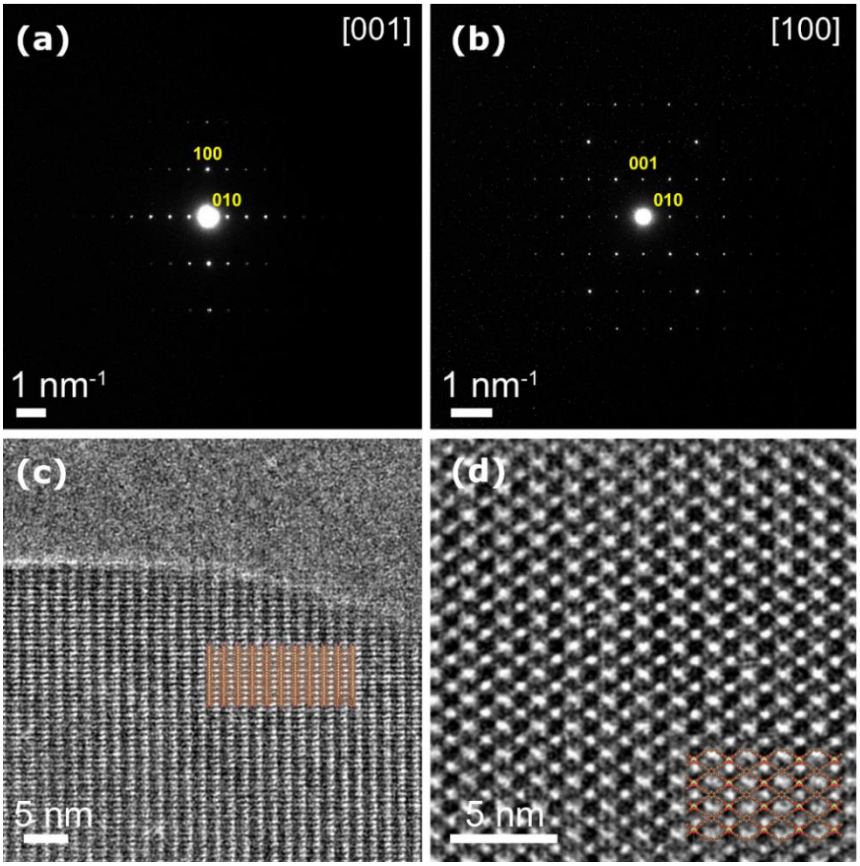

Fig. S7. (a – b) Selected area electron diffraction patterns and (c – d) the corresponding high-resolution TEM images of Ga-TCPB with inserts of the structure model.

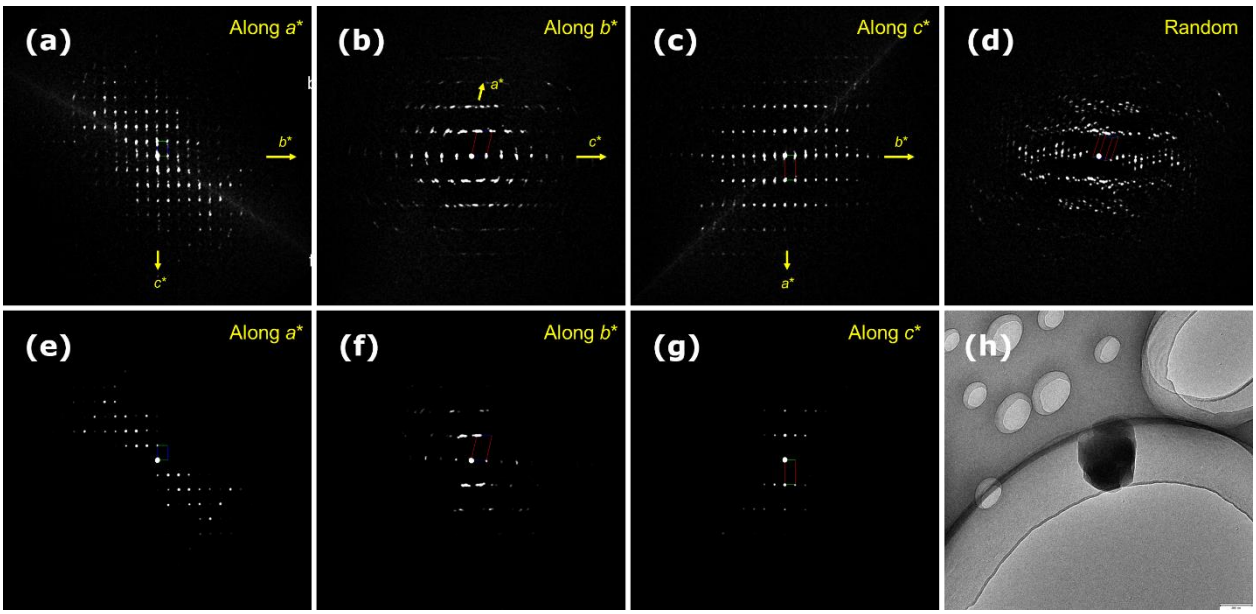

Fig. S8. (a – d) projection view of the 3D reciprocal lattice of Ga-TCPB, (e – g) 2D slices from the reconstructed 3D reciprocal lattice as obtained from the 3D ED data, and (h) low magnification bright-field image of the crystal.

Table S1. 3D crystallographic data and refinement details of V- and Ga-based MOFs.

	V-TBAPy	**Ga-TBAPy**	**V-TCPB**	**Ga-TCPB**
Composition	V_2O_2(TBAPy)	$Ga_2(OH)_2$(TBAPy)	V_2O_2(TCPB)	$Ga_2(OH)_2$(TCPB)
Crystal system	Monoclinic	Monoclinic	Orthorhombic	Monoclinic
Space group	*P2/m*	*P2/m*	*Pcma*	*P2/m*
a (Å)	6.760	6.698	6.496	6.504
b (Å)	15.696	15.321	15.835	15.971
c (Å)	15.638	16.095	21.590	10.970
α (˚)	90	90	90	90
β (˚)	103.4	102.8	90	103.4
γ (˚)	90	90	90	90
Volume (Å^3)	1614.1	1610.6	2220.7	1108.5
D_c (g cm^{-3})	0.813	0.854	1.029	1.060
Wavelength λ (Å)	0.02508 Å	0.02508 Å	0.02508 Å	0.02508 Å
Completeness (%)	89.81	89.95	81.62	67.41
Resolution (Å)	0.79 Å	0.90 Å	0.74 Å	0.75 Å
R_{int}	0.2861	0.2904	0.1464	0.0907
No. of symmetry independent reflections	3235	2082	2411	1940
R_1	0.3540	-	0.2649	0.1798
wR_2	0.6919	-	0.5788	0.5143
GooF	2.135	-	1.963	1.373

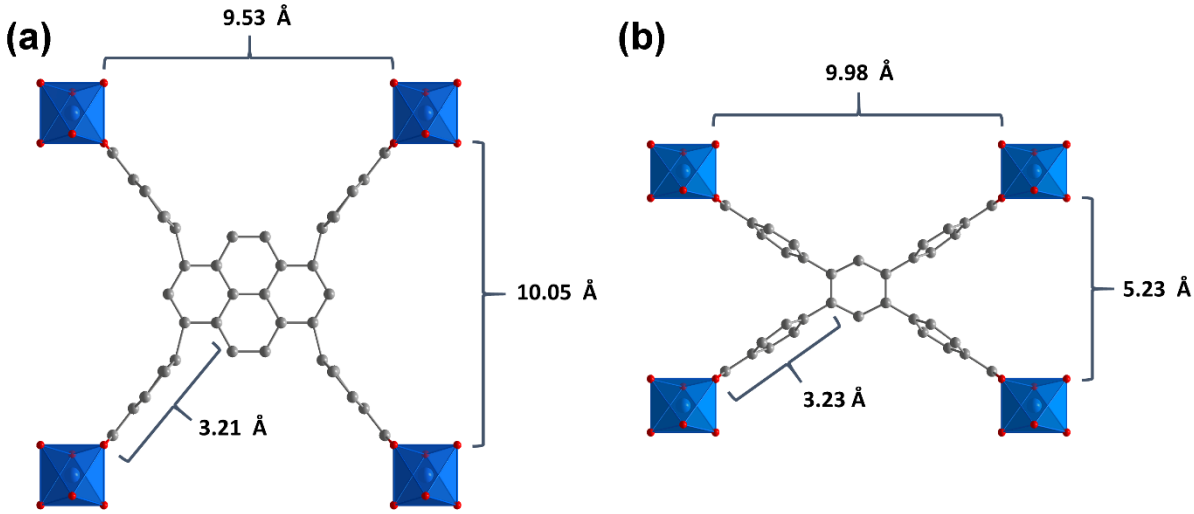

Fig. S9. Summary of dimensional differences between TBAPy- and TCPB-linkers in Ga-TBAPy and Ga-TCPB.

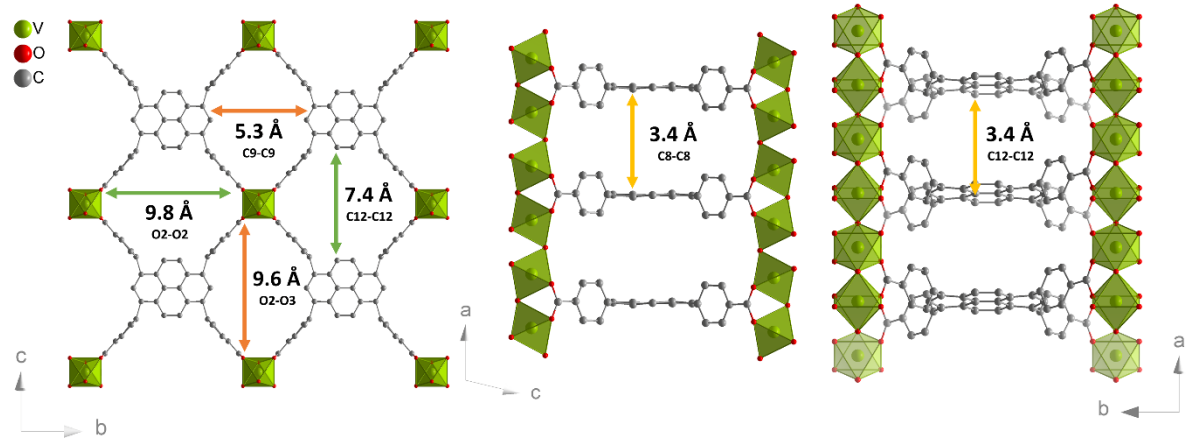

Fig. S10. Crystal structure of V-TBAPy as viewed along [001], [010], and [001] along with estimated pore diameters obtained by taking the van der Waals radii of the atoms into account.

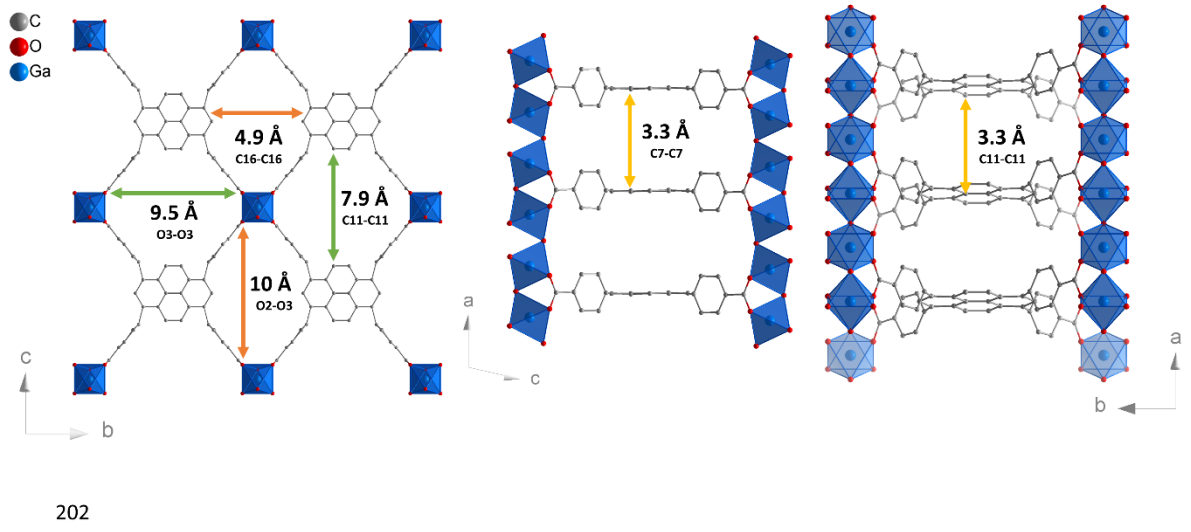

202

Fig. S11. Crystal structure of Ga-TBAPy as viewed along [001], [010], and [001] along with estimated pore diameters obtained by taking the van der Waals radii of the atoms into account.

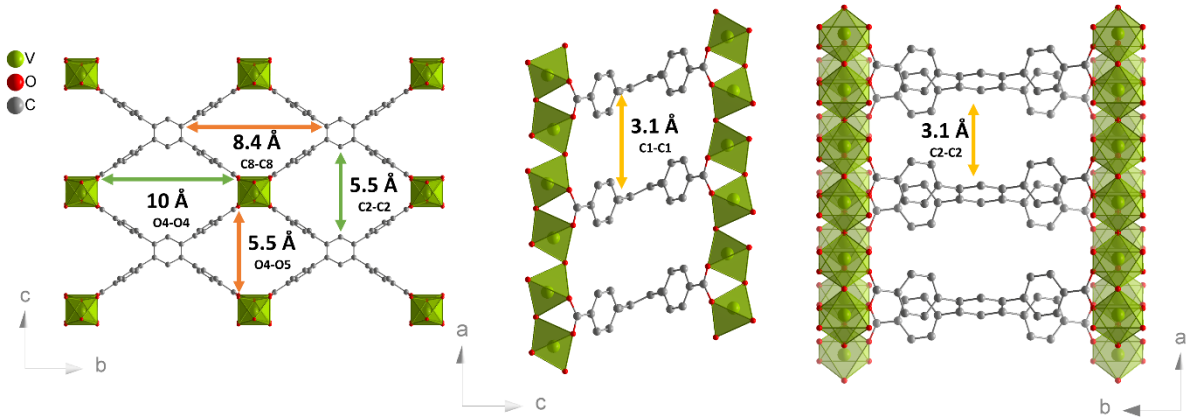

Fig. S12. Crystal structure of Ga-TCPB as viewed along [001], [010], and [001] along with estimated pore diameters obtained by taking the van der Waals radii of the atoms into account.

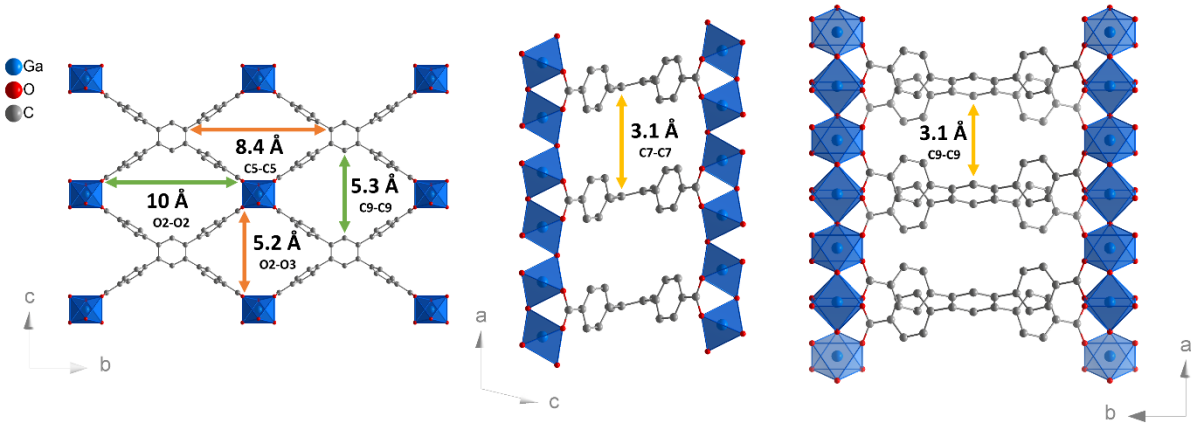

Fig. S13. Crystal structure of V-TCPB as viewed along [001], [010], and [001] along with estimated pore diameters obtained by taking the van der Waals radii of the atoms into account.

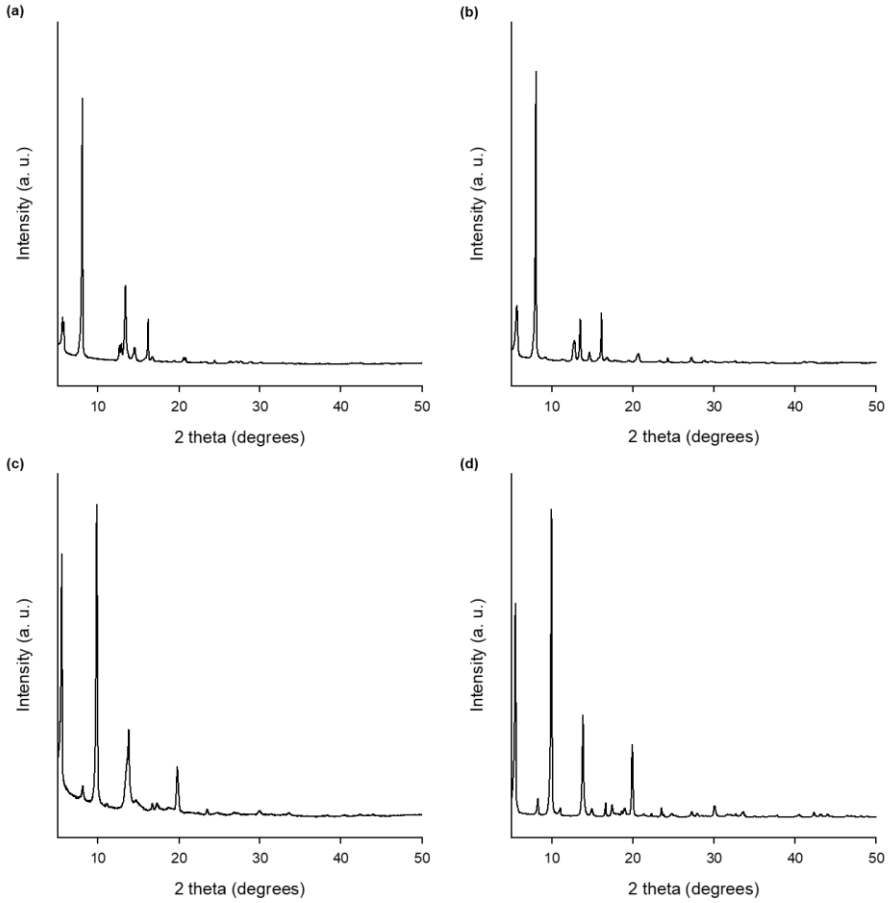

Fig. S14. Powder X-ray diffraction (λ = 1.5418 Å) patterns of (a) V-TBAPy, (b) Ga-TBAPy, (c) V-TCPB, and (d) Ga-TCPB.

Table S2. Atomic parameters obtained from Rietveld refinement of V-TBAPy[a].

Atom	Occupancy	*x*	*y*	*z*	U_{iso} (Å^2)
V1	1.0	0	0	0.5	0.024 (2)[b]
V2	1.0	0.5	0	0.5	0.024 (2)[b]
O1	1.0	0.781 (8)	0	0.556 (7)	0.02 (1)[b]
O2	1.0	0.890 (4)	0.894 (6)	0.433 (5)	0.02 (1)[b]
O3	1.0	0.610 (4)	0.923 (8)	0.403 (9)	0.02 (1)[b]
C1	1.0	0.740 (3)	0.842 (3)	0.393 (4)	0.011 (7)[b]
C2	1.0	0.768 (6)	0.7915 (13)	0.3151 (13)	0.011 (7)[b]
C3	1.0	0.758 (4)	0.8318 (13)	0.237 (2)	0.011 (7)[b]
C4	1.0	0.587 (4)	0.8182 (13)	0.165 (3)	0.011 (7)[b]
C5	1.0	0.539 (8)	0.7265 (13)	0.1600 (14)	0.011 (7)[b]
C6	1.0	0.557 (7)	0.6824 (16)	0.241 (2)	0.011 (7)[b]
C7	1.0	0.671 (11)	0.717 (2)	0.3173 (12)	0.011 (7)[b]
C8	1.0	0.550 (5)	0.6807 (9)	0.0826 (9)	0.011 (7)[b]
C9	1.0	0.5	0.722 (3)	0	0.011 (7)[b]
C10	1.0	0.5	0.5442 (15)	0.5	0.011 (7)[b]
C11	1.0	0.542 (12)	0.5900 (6)	0.0822 (7)	0.011 (7)[b]
C12	1.0	0.570 (4)	0.546 (2)	0.1608 (19)	0.011 (7)[b]

[a]The chemical composition of V-TBAPy for refinement is $V_2O_2(C_{44}O_8)$. Lattice constants are *a* = 6.754(7) Å, *b* = 15.71(3) Å, *c* = 15.66(3) Å, α = γ = 90 °, β = 103.2(2) °, resulting in *V* = 1619(5) Å^3. Agreement indices are *GoF* = 2.66, R_{wp} = 8.94. [b]Atomic displacement parameters (U_{iso}) of vanadium, oxygen, and carbon atoms in the framework are refined as a single parameter of each element.

Table S3. Atomic parameters obtained from Rietveld refinement of Ga-TBAPy[a].

Atom	Occupancy	*x*	*y*	*z*	U_{iso} (Å^2)
V1	1.0	0	0	0.5	0.005 (4)[b]
V2	1.0	0.5	0	0.5	0.005 (4)[b]
O1	1.0	0.778 (7)	0	0.556 (7)	0.031 (2)[b]
O2	1.0	0.890 (4)	0.895 (11)	0.420 (7)	0.031 (2)[b]
O3	1.0	0.530 (4)	0.911 (8)	0.403 (9)	0.031 (2)[b]
C1	1.0	0.701 (6)	0.857 (4)	0.375 (3)	0.027 (7)[b]
C2	1.0	0.699 (3)	0.8121 (14)	0.2978 (11)	0.027 (7)[b]
C3	1.0	0.894 (2)	0.762 (2)	0.194 (2)	0.027 (7)[b]
C4	1.0	0.587 (4)	0.8182 (13)	0.165 (3)	0.027 (7)[b]
C5	1.0	0.705 (5)	0.7244 (12)	0.1468 (13)	0.027 (7)[b]
C6	1.0	0.550 (3)	0.7083 (17)	0.194 (2)	0.027 (7)[b]
C7	1.0	0.549 (3)	0.754 (3)	0.2687 (14)	0.027 (7)[b]
C8	1.0	0.567 (3)	0.6829 (8)	0.0788 (8)	0.027 (7)[b]
C9	1.0	0.5	0.728 (4)	0	0.027 (7)[b]
C10	1.0	0.5	0.5452 (12)	0.5	0.027 (7)[b]
C11	1.0	0.543 (5)	0.5914 (5)	0.0787 (6)	0.027 (7)[b]
C12	1.0	0.567 (16)	0.543)	0.1558 (15)	0.027 (7)[b]

[a]The chemical composition of Ga-TBAPy for refinement is $Ga_2O_2(C_{44}O_8)$. Lattice constants are *a* = 6.697(5) Å, *b* = 15.366(17) Å, *c* = 16.01(2) Å, α = γ = 90 °, β = 101.5(1) °, resulting in *V* = 1615(3) Å^3. Agreement indices are *GoF* = 3.38, R_{wp} = 9.43. [b]The atomic displacement parameters (U_{iso}) of gallium, oxygen, and carbon atoms in the framework are refined as a single parameter of each element.

Table S4. Atomic parameters obtained from Rietveld refinement of V-TCPB[a].

Atom	Occupancy	*x*	*y*	*z*	U_{iso} (Å^2)
V1	1.0	0.310 (3)	0	0.743 (6)	0.08 (7)
O1	1.0	0.310 (2)	0.907 (17)	0.809 (9)	0.02 (8)[b]
O2	1.0	0.550 (5)	0	0.810 (3)	0.02 (8)[b]
O3	1.0	0.020 (5)	0.930 (2)	0.800 (11)	0.02 (8)[b]
C1	1.0	0.137 (4)	0.890 (3)	0.846 (4)	0.020 (13)[b]
C2	1.0	0.097 (3)	0.8097 (15)	0.871 (3)	0.020 (13)[b]
C3	1.0	0.020 (3)	0.6536 (11)	0.9270 (16)	0.020 (13)[b]
C4	1.0	0.252 (2)	0.757 (3)	0.890 (5)	0.020 (13)[b]
C5	1.0	0.213 (3)	0.6777 (15)	0.915 (3)	0.020 (13)[b]
C6	1.0	-0.093 (3)	0.7902 (18)	0.892 (4)	0.020 (13)[b]
C7	1.0	-0.132 (3)	0.711 (2)	0.918 (4)	0.020 (13)[b]
C8	1.0	-0.019 (5)	0.583 (2)	0.9649 (13)	0.020 (13)[b]
C9	1.0	0	0.5	0.941 (2)	0.020 (13)[b]

[a]The chemical composition of V-TCPB for refinement is $V_2O_2(C_{34}O_8)$. Lattice constants are *a* = 6.822(13) Å, *b* = 15.84(5) Å, *c* = 21.59(3) Å, α = β = γ = 90 °, resulting in *V* = 2333(9) Å^3. Agreement indices are *GoF* = 2.14, R_{wp} = 7.64. [b]The atomic displacement parameters (U_{iso}) of vanadium, oxygen, and carbon atoms in the framework are refined as a single parameter of each element.

Table S5. Atomic parameters obtained from Rietveld refinement of Ga-TCPB[a].

Atom	Occupancy	*x*	*y*	*z*	U_{iso} (Å^2)
Ga1	1.0	0	0	0.5	0.006 (4)[b]
Ga2	1.0	0.5	0	0.5	0.006 (2)[b]
O1	1.0	0.781 (2)	0	-0.390 (3)	0.02 (1)[b]
O2	1.0	0.120 (4)	-0.082 (6)	-0.366 (3)	0.02 (1)[b]
O3	1.0	0.460 (2)	-0.093 (9)	-0.389 (9)	0.02 (1)[b]
C1	1.0	0.326 (3)	-0.120 (3)	-0.328 (5)	0.004 (5)[b]
C2	1.0	0.3763 (19)	-0.1911 (11)	-0.254 (2)	0.004 (5)[b]
C3	1.0	0.219 (2)	-0.2320 (13)	-0.216 (3)	0.004 (5)[b]
C4	1.0	0.573 (2)	-0.2302 (13)	-0.234 (3)	0.004 (5)[b]
C5	1.0	0.606 (2)	-0.3109 (12)	-0.184 (3)	0.004 (5)[b]
C6	1.0	0.255 (2)	-0.3128 (12)	-0.166 (2)	0.004 (5)[b]
C7	1.0	0.4529 (18)	-0.3491 (8)	-0.1415 (16)	0.004 (5)[b]
C8	1.0	0.501 (3)	-0.4233 (18)	-0.069 (2)	0.004 (5)[b]
C9	1.0	0.415(18)	0.5	-0.122(4)	0.04)[b]

[a]The chemical composition of Ga-TCPB for refinement is $Ga_2O_2(C_{34}O_8)$. Lattice constants are a = 6.695(5) Å, b = 16.05(2) Å, c = 11.228(10) Å, α = γ = 90 °, β = 107.84(11) °, resulting in V = 1149(2) Å^3. Agreement indices are *GoF* = 3.27, R_{wp} = 9.59. [b] The atomic displacement parameters (U_{iso}) of gallium, oxygen, and carbon atoms in the framework are refined as a single parameter of each element.

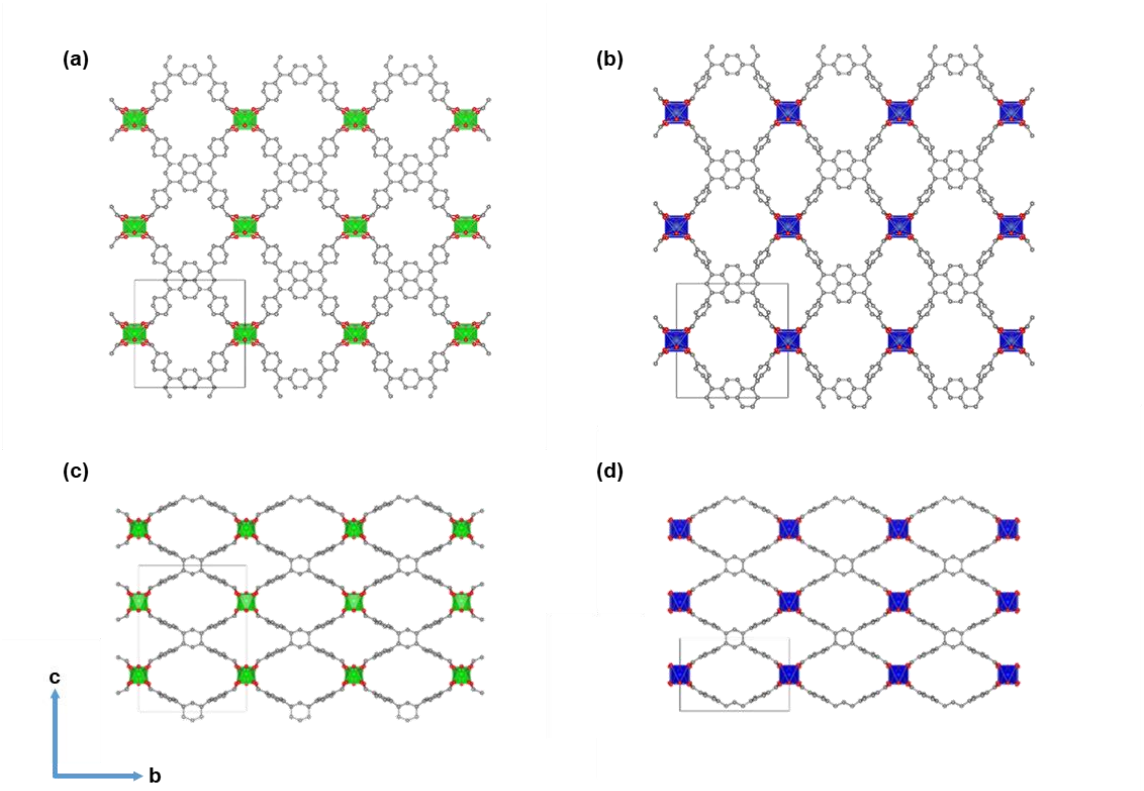

Fig. S15. Atomic configuration of (a) V-TBAPy, (b) Ga-TBAPy, (c) V-TCPB, and (d) Ga-TCPB along [100], drawn based on the crystal structure as determined by Rietveld refinement: V and VO_6 unit (green), Ga and GaO_6 unit (blue), O (red), and C (grey).

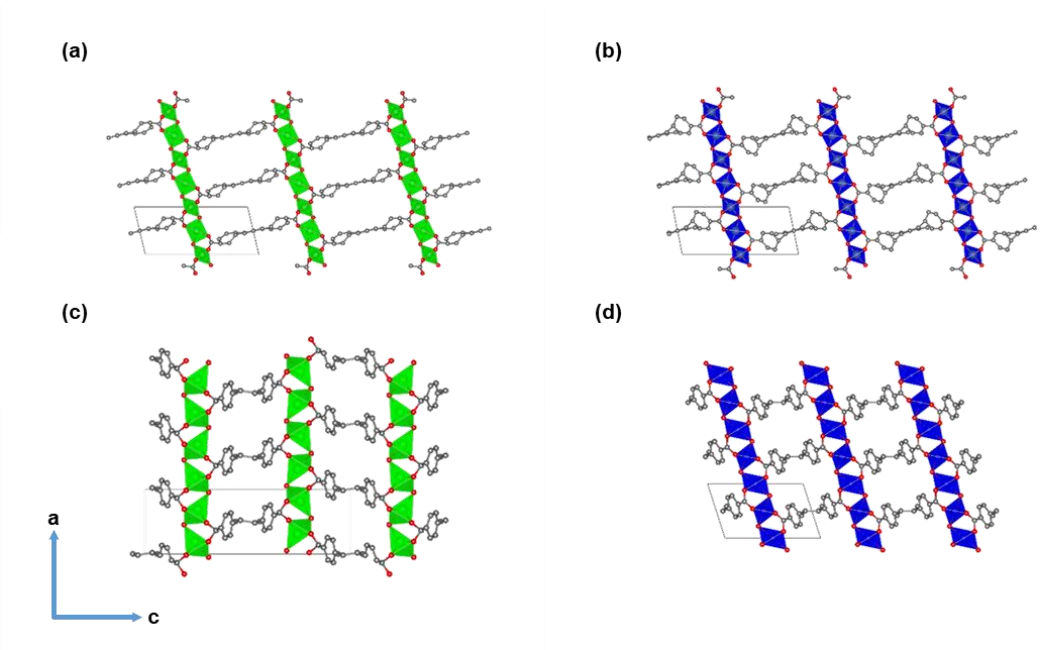

Fig. S16. Atomic configuration of (a) V-TBAPy, (b) Ga-TBAPy, (c) V-TCPB, and (d) Ga-TCPB along [010], drawn based on the crystal structure as determined by Rietveld refinement: V and VO_6 unit (green), Ga and GaO_6 unit (blue), O (red), and C (grey).

Section S3. X-ray photoelectron spectroscopy

Survey and high-resolution core-level X-ray photoelectron spectroscopy (XPS) spectra were recorded on an Ulvac-PHI Quantera II XPS Scanning Microprobe using monochromatic Al Kα as an X-ray source. All measurements were conducted under a constant exposure of low-energy electrons and argon ions in order to avoid charge build-up. Both the core-level spectra of V2p could be deconvoluted as two single-component peaks, indicating that the MOFs contain a single vanadium species. Furthermore, binding energies for $V2p_{3/2}$ and $V2p_{1/2}$ (Table S6) was measured to be 515.78 eV, 523.13 eV and 515.95 eV, 523.30 eV for V-TBAPy and V-TCPB, respectively, and a difference in binding energy between O1s and $V2p_{3/2}$ was calculated to be 14.60 and 14.61, indicating that the oxidation state of vanadium in both MOFs is V(IV)[10, 11].

The presence of Si in the survey spectra comes from the substrates (silicon wafers) that the MOFs were placed on during the measurements.

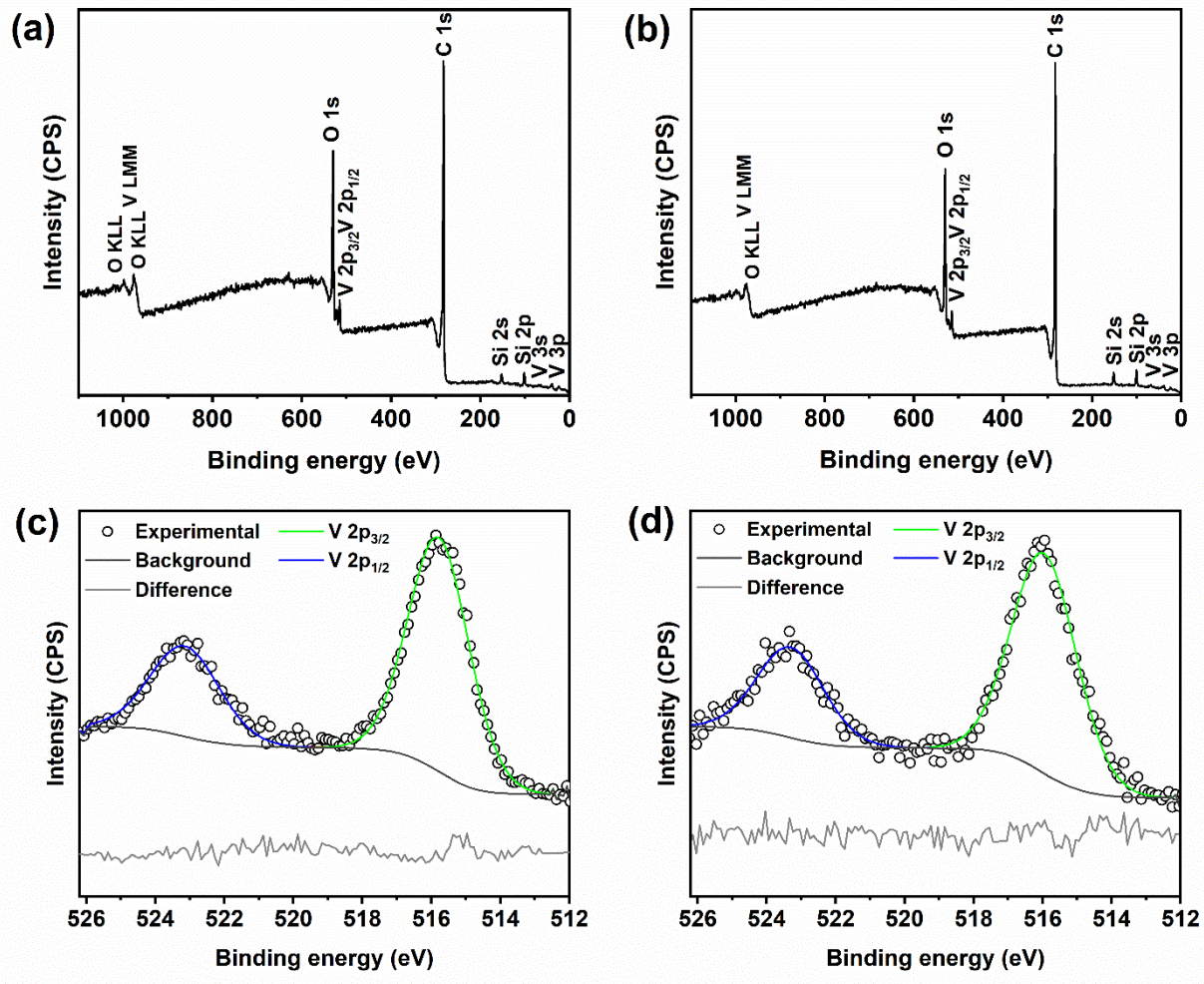

Fig. S17. XPS (a – b) survey and core-level (c – d) spectra of (a)/(c) V-TBAPy and (b)/(d) V-TCPB.

Table S6. Summary of V2p and O1s peak fit parameters for V-TBAPy and V-TCPB.

Sample / Binding energy (eV)	V-TBAPy	V-TCPB
$V2p_{3/2}$	515.78	515.95
$V2p_{1/2}$	523.13	523.30
O1s	530.38	530.50
Δ($V2p_{1/2}$ and $V2p_{3/2}$)	7.35	7.35
Δ(O1s and $V2p_{3/2}$)	14.60	14.61

Section S4. Stability study

The chemical stability of the as-synthesized MOFs was evaluated by soaking 8 mg of each material in 5 ml of the following solutions; 1 M HCl, deionized water, 1 M NaOH, MeOH, EtOH, toluene, and acetone, for 24 h whilst stirring at 300 rpm. The materials were thereafter collected by centrifugation at 3,800 rpm for 10 min and analyzed using PXRD, Figure S17 – S18. All samples can be observed to have low stability in strongly acidic or basic solutions after 24 h. The frameworks can be seen to either partially decompose or fully dissolve after having been left stirring in these solutions, indicating that the coordination between the metal ions and organic linkers may be vulnerable to gradual replacement in these conditions. The structural stability of MOFs in all other solutions and solvents was found to be high, with only minor changes in crystallinity possibly connected to the adsorption of molecules into the frameworks. The thermal stability of MOFs was studied in air (60 ml min^{-1} flow-rate) using thermogravimetric analysis (TGA), Figure S19. All samples were found to remain stable up to 350 ˚C, with the Ga-based MOFs showing significantly higher thermal stability (decomposing at approx. 450 ˚C).

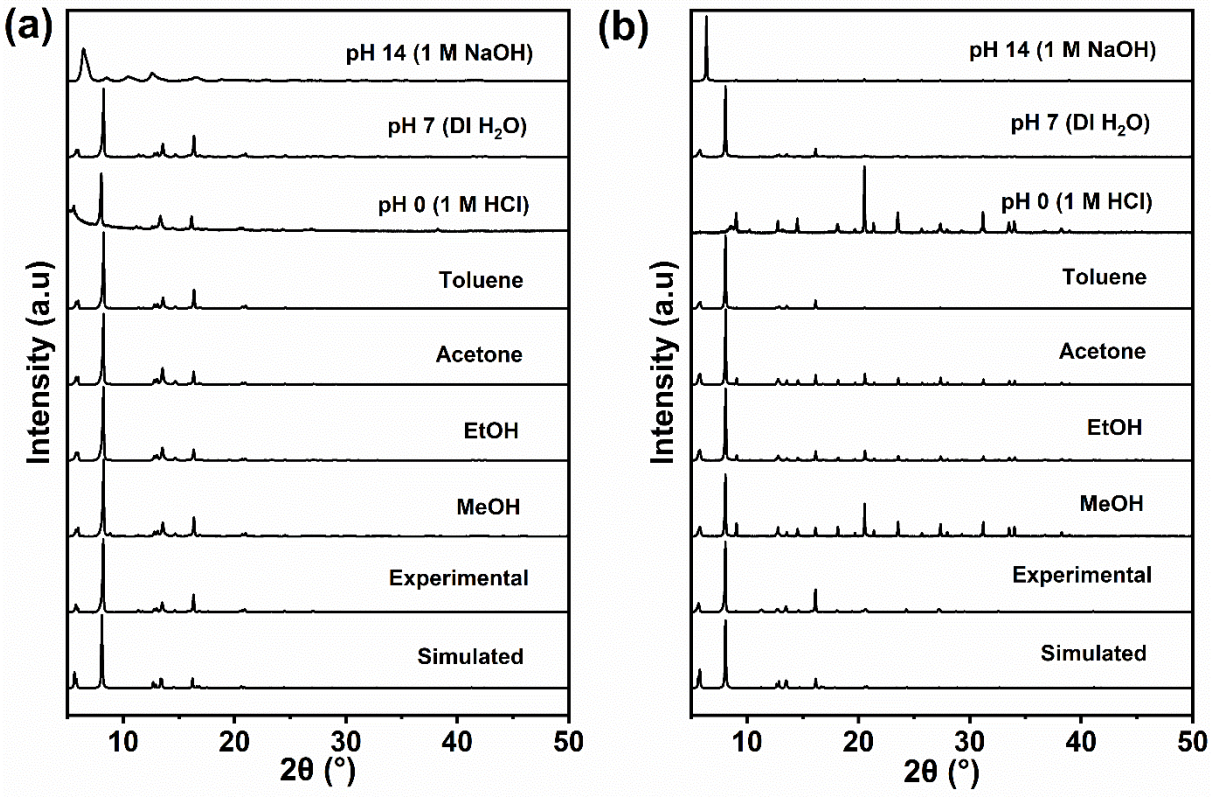

Fig. S18. X-ray powder diffractograms of (a) V-TBAPy and (b) Ga-TBAPy

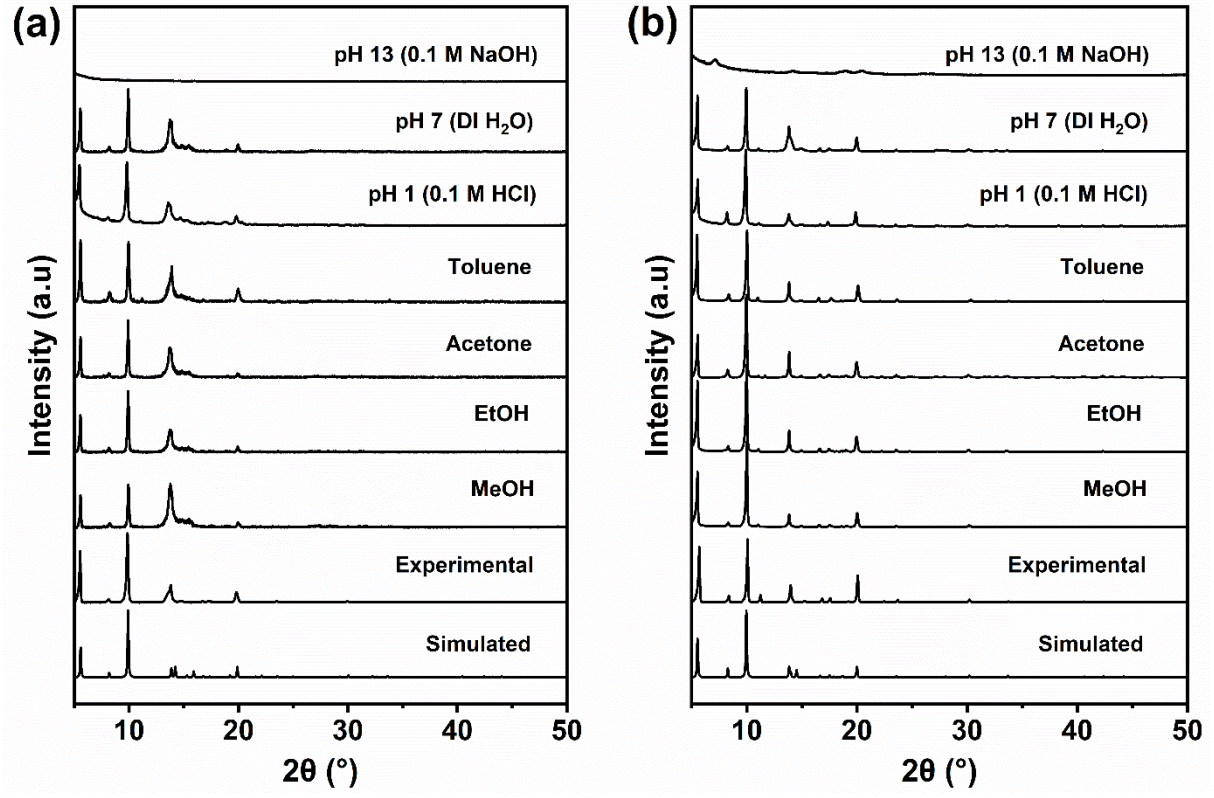

Fig. S19. X-ray powder diffractograms of (a) V-TCPB and (b) Ga-TCPB

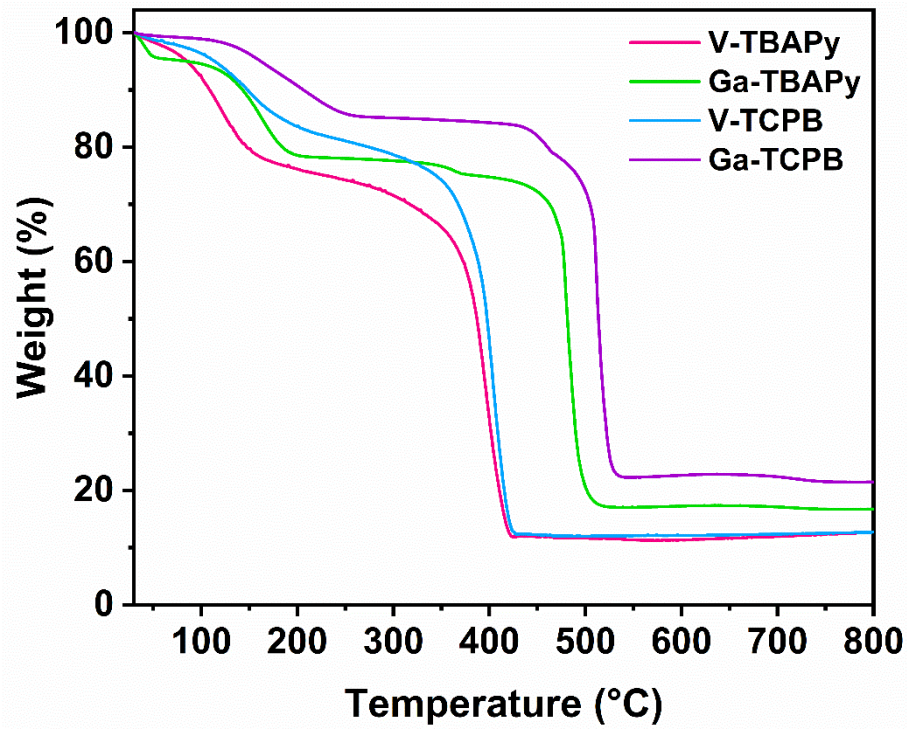

Fig. S20. Thermogravimetric decomposition profiles of Ga- and V-based MOFs.

Section S5. Scanning electron microscopy images

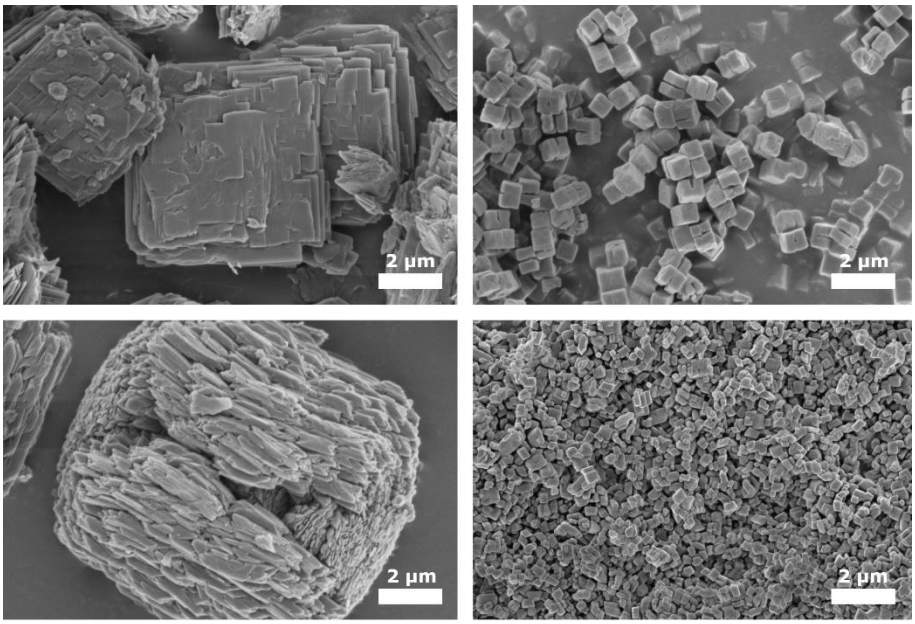

Fig. S21. Scanning electron microscopy images of (a) V-TBAPy, (b) Ga-TBAPy, (c) V-TCPB, and (d) Ga-TCPB.

Section S6. Porosity and gas sorption

Gas sorption experiments were performed using a Micromeritics ASAP 2020 surface area analyzer (Norcross, GA, USA). All samples were pre-treated at 423 K for 3 h under a dynamic vacuum (1×10^{-4} Pa) prior to analysis. Brunauer-Emette-Teller (BET) and Langmuir-specific surface areas were calculated from N_2 adsorption isotherms recorded at 77 K. Pore size distributions were estimated using the Density Functional Theory (DFT) function in the Micromerities MicroActive software using the N_2 adsorption isotherms, the slit pore model for N_2 was used for these calculations. SF_6, CO_2, CH_4, and N_2 sorption isotherms at 283 - 303 K were also recorded using the Micromeritics ASAP 2020 surface area analyzer with an insulating water bath. Gravimetric gas adsorption profiles were obtained using a Mettler Toledo TGA/DSC 3+ (Schwerzenbach, Switzerland) using N_2 as purge gas and SF_6 or CO_2 as measurement gas. All experiments were carried out on approx. 10 mg of material degassed at 423 K for 30 min in a N_2 atmosphere (50 ml min^{-1} flow-rate) before the sample were subjected to SF_6 or CO_2 at 303 K for up to 30 min (50 ml min^{-1} flow-rate). Temperature-swing adsorption experiments were carried out under the same conditions, however using a shorter degas time of 12 min in-between each cycle.

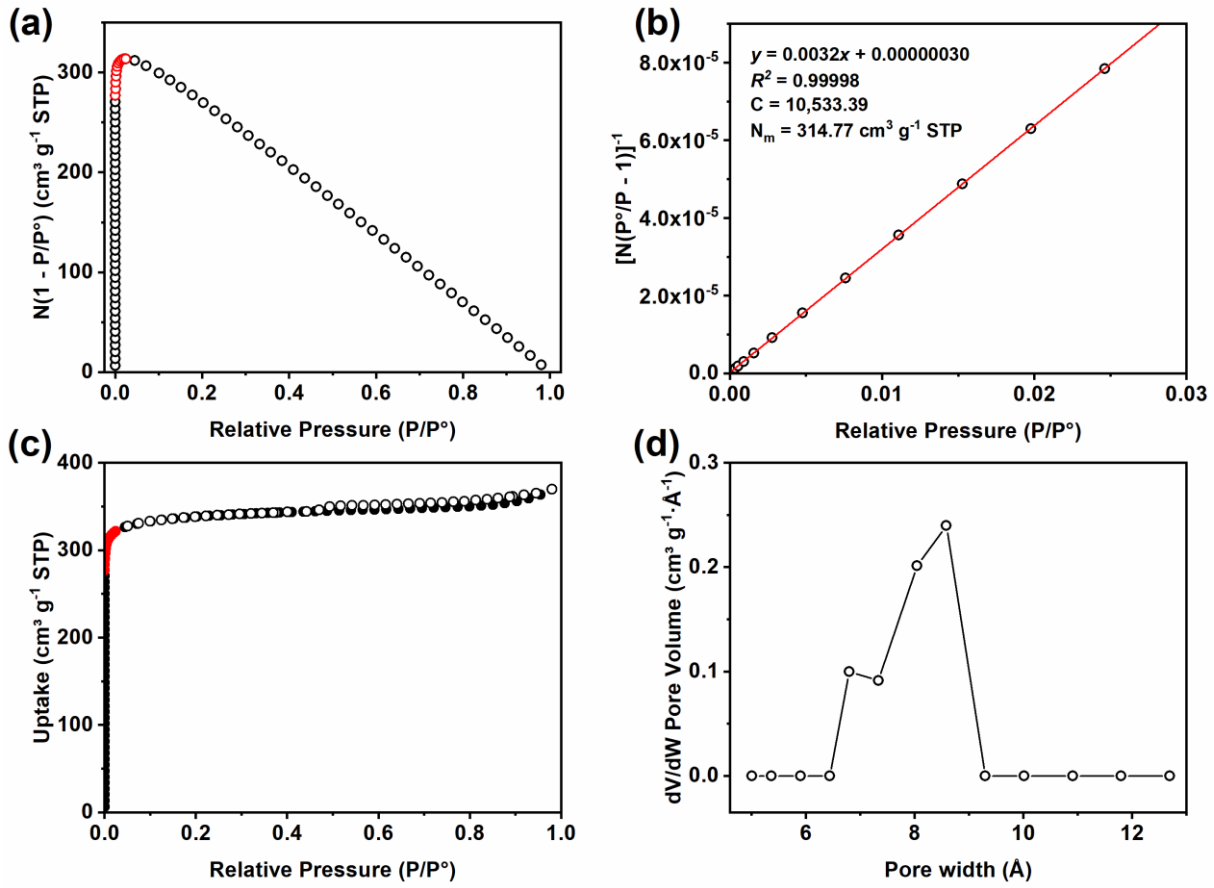

Fig. S22. (a) Rouquerol plot, (b) BET surface area plot showing selected points for satisfying the Rouquerol criterion, (c) N_2 sorption isotherm recorded at 77 K, and (d) corresponding density-functional theory pore size distributions for V-TBAPy. Red hollow and solid spheres correspond to selected points used for calculating the BET surface area of the material. Black-filled and hollow spheres denote the adsorption and desorption branches of the N_2 isotherm, respectively.

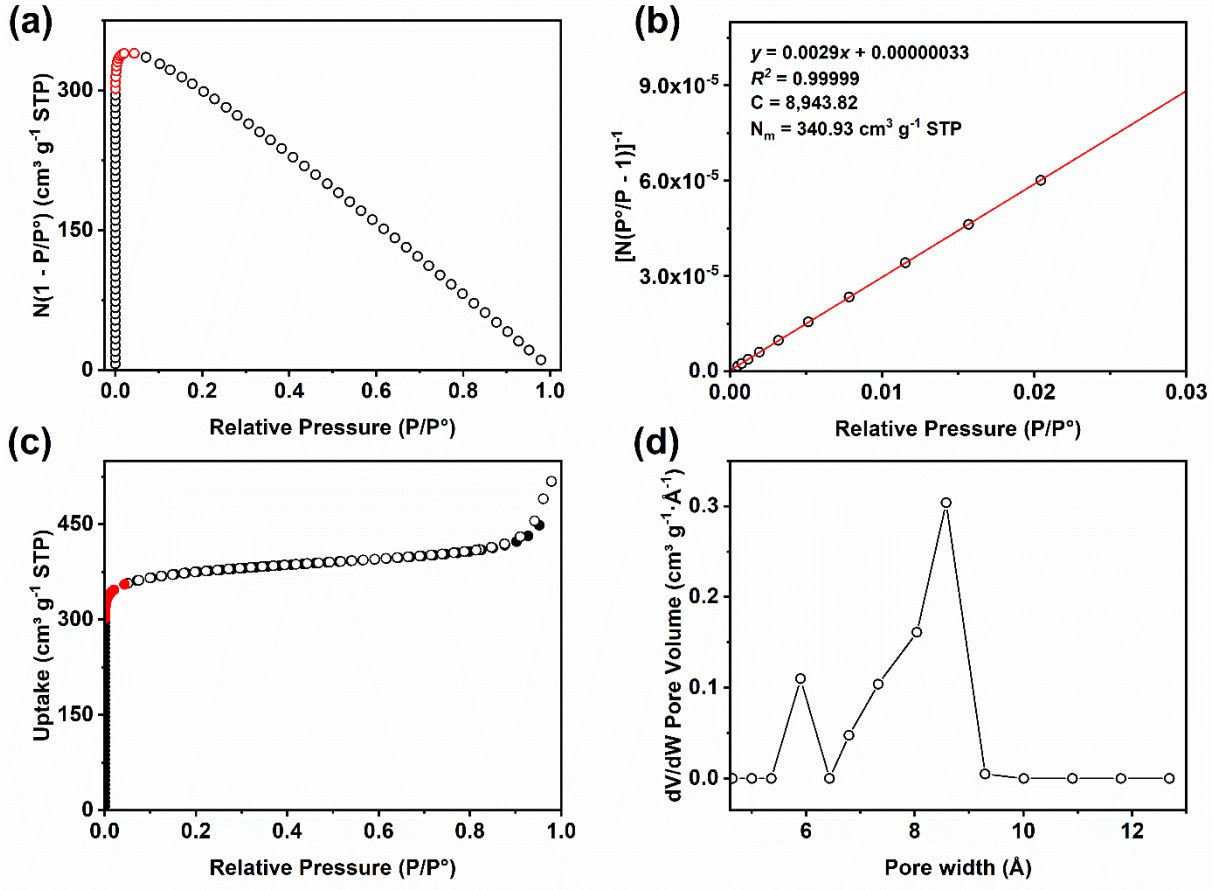

Fig. S23. (a) Rouquerol plot, (b) BET surface area plot showing selected points for satisfying the Rouquerol criterion, (c) N_2 sorption isotherm recorded at 77 K, and (d) corresponding density-functional theory pore size distributions for Ga-TBAPy. Red hollow and solid spheres correspond to selected points used for calculating the BET surface area of the material. Black-filled and hollow spheres denote the adsorption and desorption branches of the N_2 isotherm, respectively.

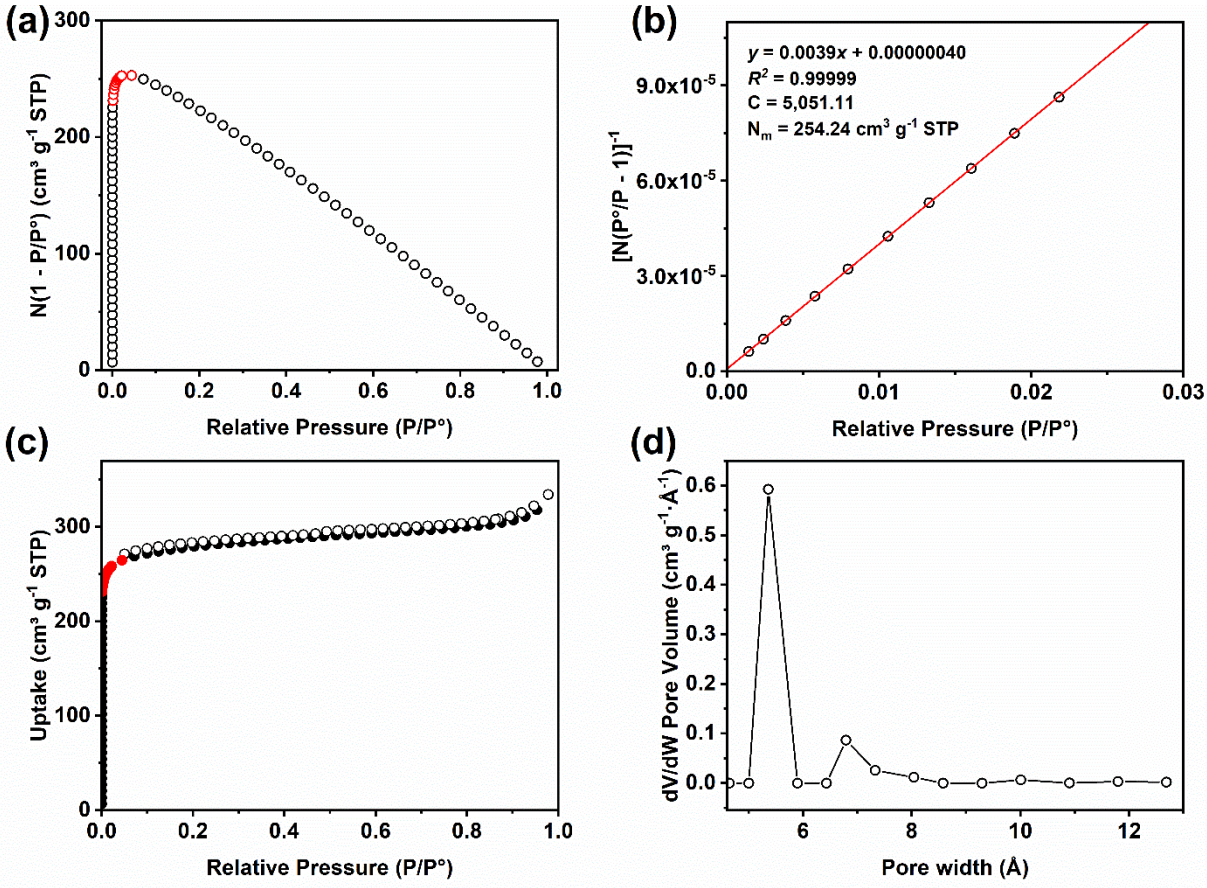

Fig. S24. (a) Rouquerol plot, (b) BET surface area plot showing selected points for satisfying the Rouquerol criterion, (c) N_2 sorption isotherm recorded at 77 K, and (d) corresponding density-functional theory pore size distributions for V-TCPB. Red hollow and solid spheres correspond to selected points used for calculating the BET surface area of the material. Black-filled and hollow spheres denote the adsorption and desorption branches of the N_2 isotherm, respectively.

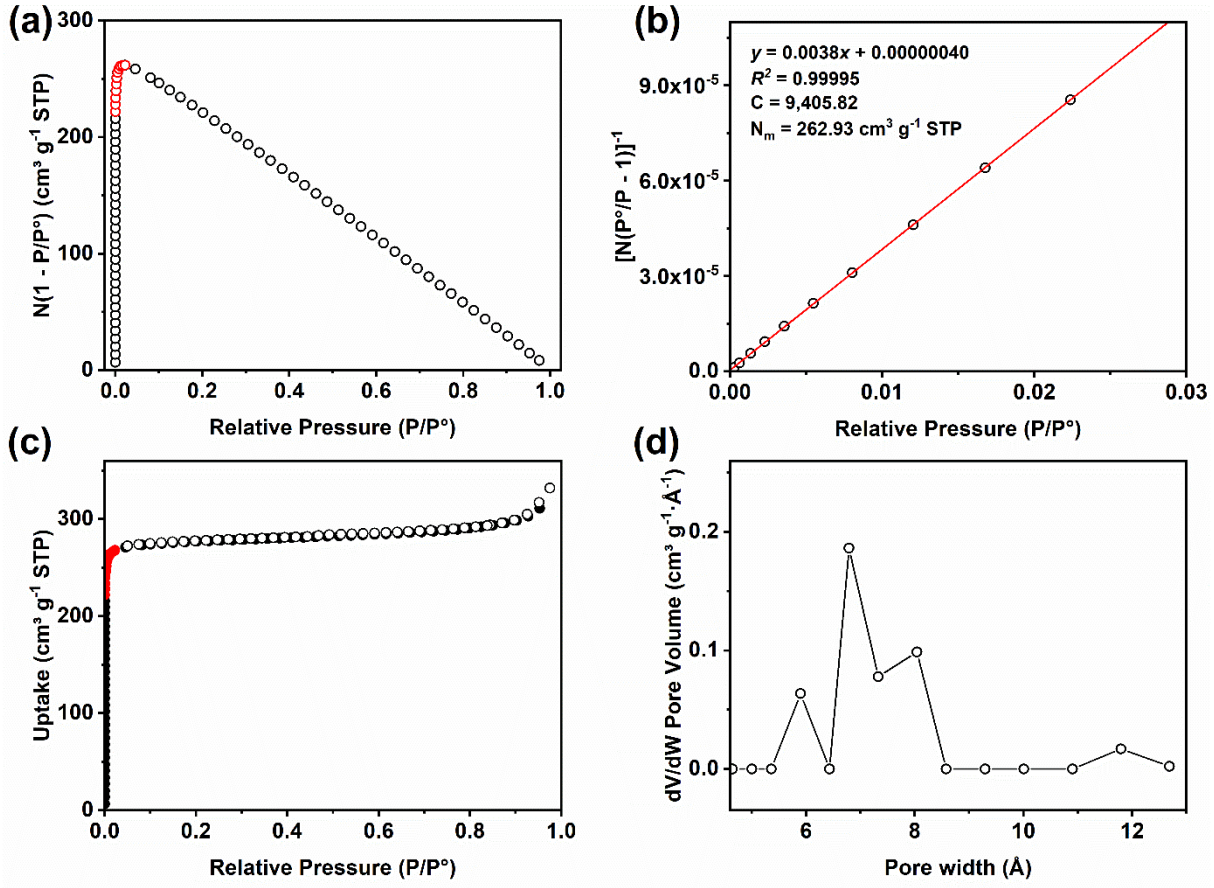

Fig. S25. (a) Rouquerol plot, (b) BET surface area plot showing selected points for satisfying the Rouquerol criterion, (c) N_2 sorption isotherm recorded at 77 K, and (d) corresponding density-functional theory pore size distributions for Ga-TCPB. Red hollow and solid spheres correspond to selected points used for calculating the BET surface area of the material. Black-filled and hollow spheres denote the adsorption and desorption branches of the N_2 isotherm, respectively.

Table S7. Summary of porosity properties of the V-TABPy, Ga-TBAPy, V-TCPB, and Ga-TCPB.

Sample	BET surface area[a] ($m^2\ g^{-1}$)	Langmuir surface area ($m^2\ g^{-1}$)	BET constant, C	Pore volume[b] ($cm^3\ g^{-1}$)	Pore size[c] (Å)
V-TBAPy	1370	1482	10,533.39	0.557	6.40, 8.60
Ga-TBAPy	1484	1646	8,943.82	0.669	5.90,8.60
V-TCPB	1107	1224	5,051.11	0.482	5.38,6.82
Ga-TCPB	1144	1209	9,405.82	0.469	5.95,6.80, 7.85

[a]Calculated from the N_2 adsorption isotherm recorded at 77 K in the P/P°-range given in Figs. S22-S25.
[b]Total pore volume estimated from the adsorption branch of the N_2 isotherm recorded at 77 K at P/P° = 0.93.
[c]Calculated by DFT from the adsorption branch of the N_2 isotherm recorded at 77 K at P/P° < 1×10^{-2} using a slit-type pore geometry.

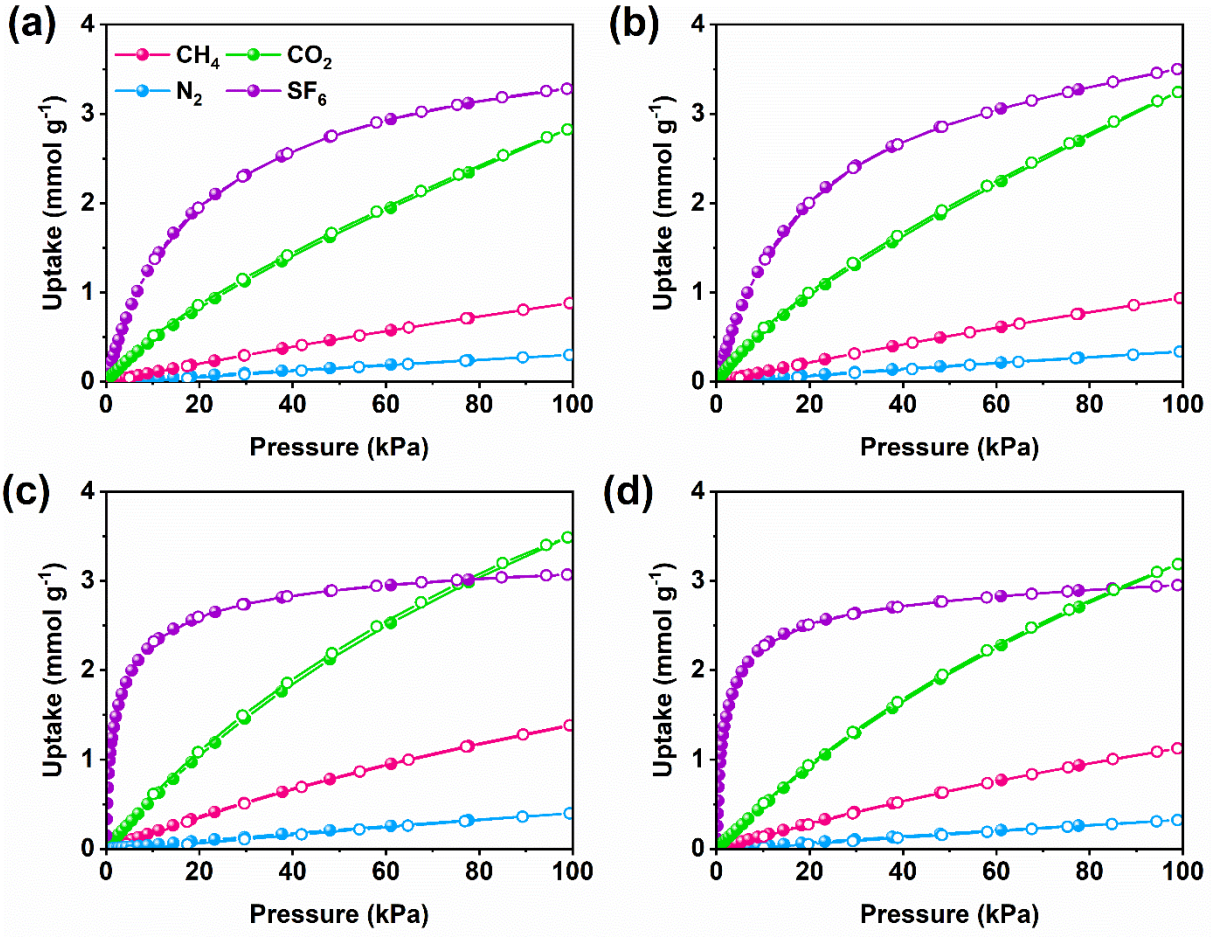

Fig. S26. CH_4, CO_2, N_2, and SF_6 sorption isotherms recorded at 293 K of (a) V-TBAPy, (b) Ga-TBAPy, (c) V-TCPB, and (d) Ga-TCPB. Filled and hollow spheres represent the adsorption and desorption isotherms, respectively.

Table S8. Uptake capacities of CH_4, CO_2, N_2, and SF_6 at 293 K and 100 kPa of V-TBAPy, Ga-TBAPy, V-TCPB, and Ga-TCPB.

Samples	CH_4 (mmol g^{-1})	CO_2 (mmol g^{-1})	N_2 (mmol g^{-1})	SF_6 (mmol g^{-1})
V-TBAPy	0.88	2.83	0.30	3.28 1.32[a]
Ga-TBAPy	0.94	3.24	0.34	3.50 1.33[a]
V-TCPB	1.38	3.49	0.40	3.07 2.29[a]
Ga-TCPB	1.13	3.19	0.32	2.95 2.25[a]

[a]Uptake at 10 kPa.

Table S9. Summary of SF_6 uptake capacities, selectivities, and enthalpies of adsorption of various MOF sorbents.

Materials	SF_6 uptake at 10 kPa (mmol g^{-1})	SF_6 uptake at 100 kPa (mmol g^{-1})	IAST selectivity (10:90) SF_6/N_2	$-\Delta H_{ads}$ (kJ mol^{-1})[a]	Ref.
Cu-MOF-NH_2	3.39	7.88	266.2	55.20	12
Zn(TMBDC)(DABCO)$_{0.5}$	2.48	4.61	219.0	45.20	13
Ni(ina)$_2$	2.39	2.84	375.1	33.40	14
V-TCPB	**2.29**	**3.07**	**360.7**	**30.48**	**This work**
Ga-TCPB	**2.26**	**2.95**	**418.5**	**30.44**	**This work**
Ni(adc)(dabco)$_{0.5}$	2.23	2.38	919.4	47.68	15
Co-MOF-74	2.09	5.34	35.1	40.00	16
Mg-MOF-74	2.04	6.42	18.9	32.00	16
Ni(3-mpba)$_2$	1.79	2.83	221.0	30.20	17
Co(3-mpba)$_2$	1.77	3.25	161.0	26.80	17
Ni(pba)$_2$	1.69	3.47	156.5	26.10	17
Zn-MOF-74	1.42	3.72	46.0	25.00	16
HKUST-1	1.41	6.71	159.4	27.73	18
Zn(DMBDC)(DABCO)$_{0.5}$	1.40	4.77	109.3	26.50	13
Ga-TBAPy	**1.33**	**3.50**	**55.4**	**27.18**	**This work**
V-TBAPy	**1.33**	**3.28**	**65.6**	**28.08**	**This work**
CAU-10-Py	1.13	1.76	203.6	32.60	19
SBMOF-1	0.93	1.02	325.0	32.50	20
UiO-66	0.82	1.67	129.9	32.38	21
UiO-66-Br_2	0.76	0.94	222.2	44.62	21
CAU-10-H	0.68	1.00	122.6	24.90	19
UiO-67	0.48	3.58	21.5	20.43	22
MIL-100(Fe)	0.30	2.59	15.8	24.19	23

[a]At zero or low coverage

Section S6.1. Isosteric enthalpies of adsorption

Isosteric enthalpies of SF_6 and CO_2 adsorption were estimated from pure-component isotherms of SF_6 or CO_2 recorded at 283 – 303 K using the Virial equation (Eq. 1)[24]:

$$\ln P = \ln N + \frac{1}{T}\sum_{i=0}^{m} a_i N^i + \sum_{j=0}^{n} b_j N^j \quad [1]$$

Where P (kPa) is the ideal gas constant, N (mmol g^{-1}) quantity of adsorbed gas at temperature T (K), a_i and b_j virial coefficients.

The isosteric enthalpy of adsorption (ΔH_{ads}) was thereafter calculated using Eq. 2:

$$\Delta H_{ads} = R\sum_{i=0}^{m} a_i N^i \quad [2]$$

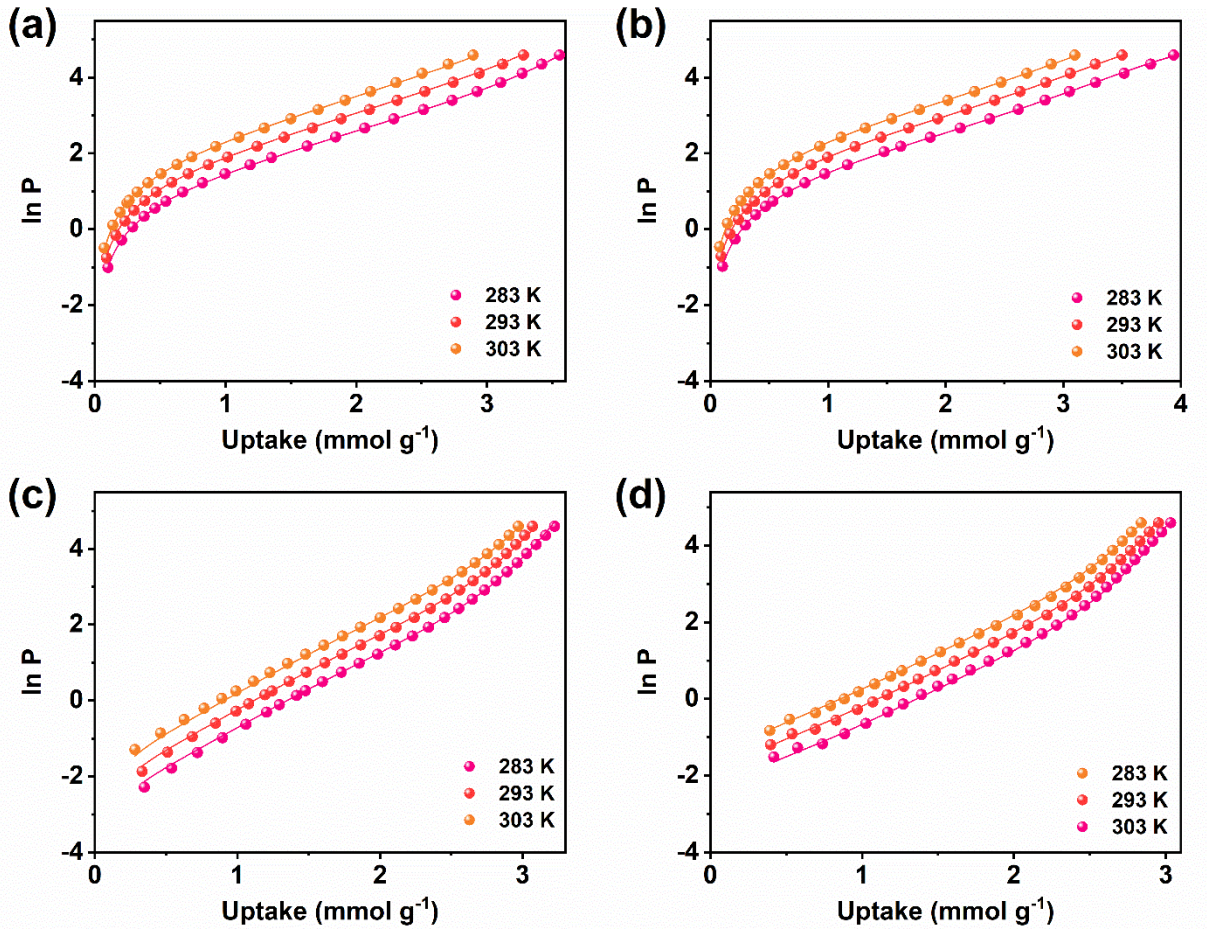

Fig S27. Virial fit of SF_6 adsorption isotherms recorded at 283 – 303 K for (a) V-TBAPy, (b) Ga-TBAPy, (c) V-TCPB, and (d) Ga-TCPB.

Table S10. Fitting parameters and virial coefficients obtained from SF_6 adsorption isotherms recorded at 283 – 303 K of V-TBAPy.

Sample	V-TBAPy ±	Ga-TBAPy	V-TCPB	Ga-TCPB
a_0	-3280.456	-3198.130	-3487.004	-3428.464
a_1	-392.009	-300.055	-909.842	-3428.464
a_2	13.265	76.659	757.361	972.760
a_3	33.483	-44.172	-305.211	-381.211
a_4	-14.937	15.391	47.576	61.515
a_5	2.208	-1.775	-	-
b_0	12.883	12.598	11.562	12.050
b_1	1.418	1.084	1.497	1.266
RMSE	0.01998	0.01455	0.05194	0.04840

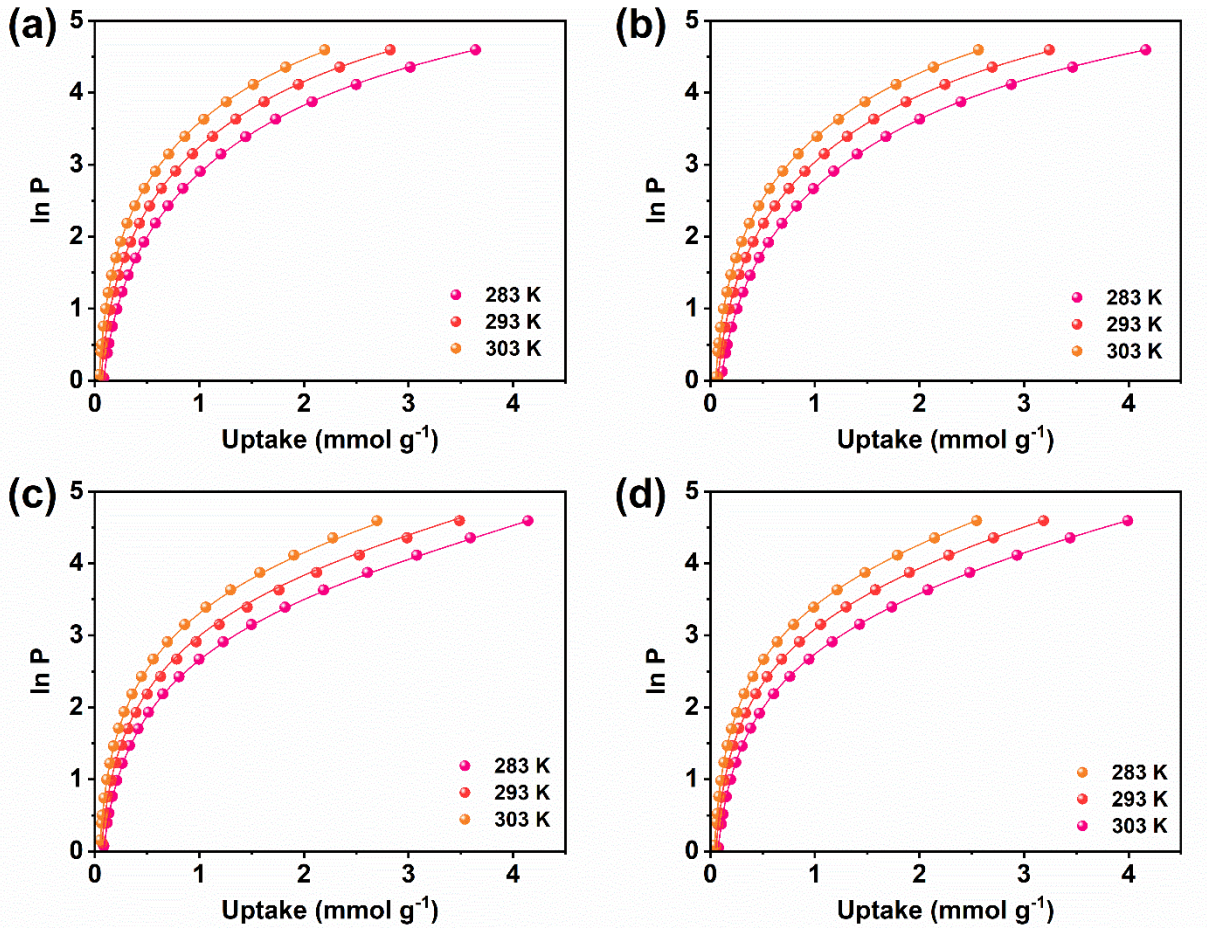

Fig S28. Virial fit of CO_2 adsorption isotherms recorded at 283 – 303 K for (a) V-TBAPy, (b) Ga-TBAPy, (c) V-TCPB, and (d) Ga-TCPB.

Table S11. Fitting parameters and virial coefficients obtained from CO_2 adsorption isotherms recorded at 283 – 303 K of V-TBAPy.

Sample	V-TBAPy	Ga-TBAPy	V-TCPB	Ga-TCPB
a_0	-3346.979	-3304.601	-2767.651	-2800.397
a_1	372.217	331.174	-2.378	-69.746
a_2	-37.975	-32.823	-7.497	5.416
a_3	3.381	2.650	1.342	-0.515
b_0	14.264	13.914	12.264	12.520
b_1	-0.748	-0.626	0.202	0.346
RMSE	0.00892	0.00667	0.03000	0.00674

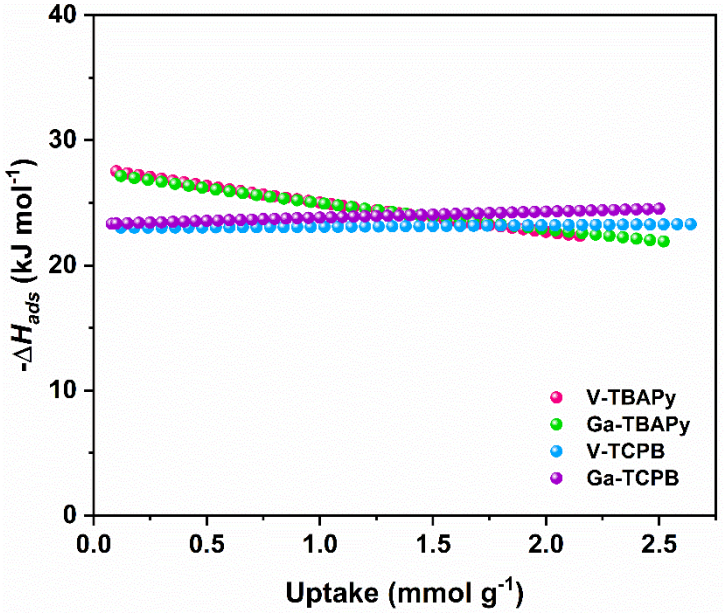

Fig. S29. Isosteric enthalpies of CO_2 adsorption ($-\Delta H_{ads}$) for V-, Ga-TBAPy and V-, Ga-TCPB.

Section S6.2. Gas selectivity

Section S6.2.1. Ideal (Henry's Law) selectivity

Ideal selectivities were calculated from pure-component CH_4, CO_2, N_2, and SF_6 isotherms at 293 K in the low-pressure region using the Henry's law constants ($s = K_{H,gas1}/K_{H,gas2}$).

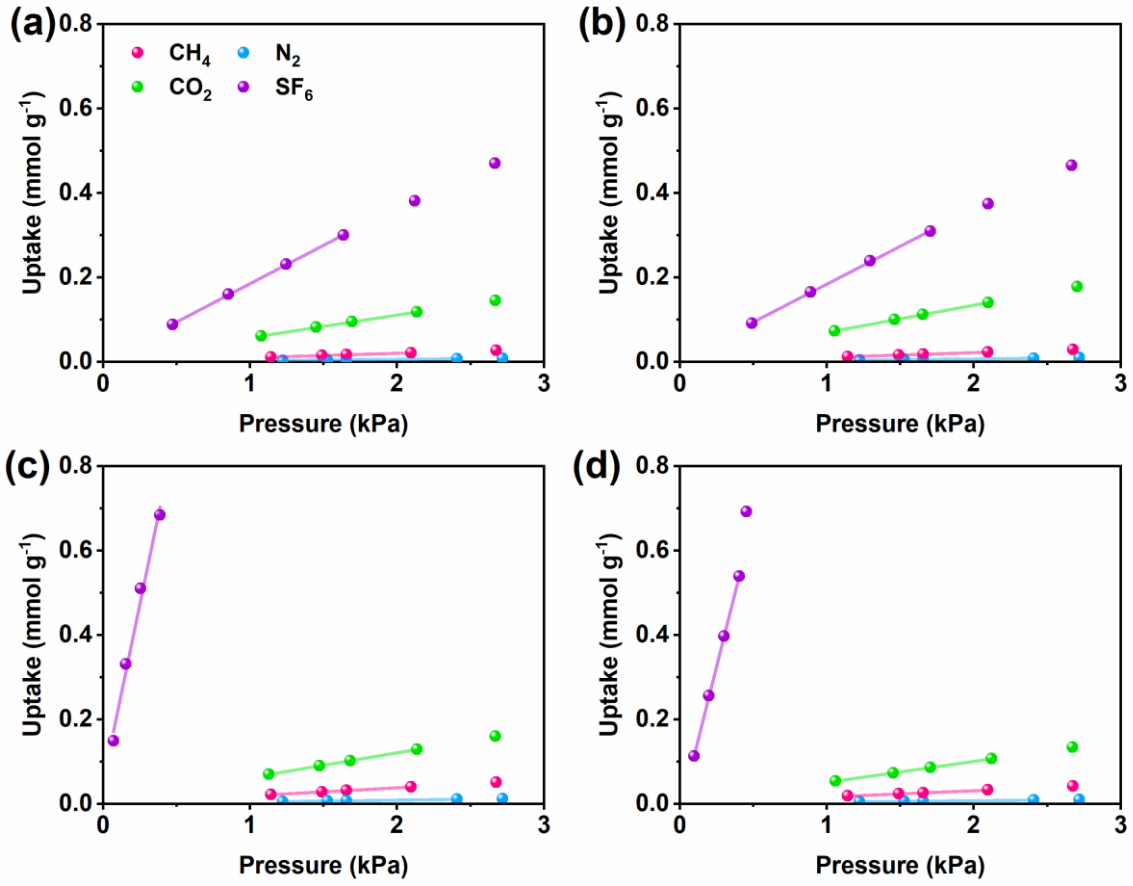

Fig S30. Linear fits of the CH_4, CO_2, N_2, and SF_6 adsorption isotherms recorded at 293 K in the low-pressure region of (a) V-TBAPy, (b) Ga-TBAPy, (c) V-TCPB, and (d) Ga-TCPB.

Table S12. Linear fitting parameters and calculated ideal SF_6/N_2, CO_2/N_2 selectivities from low-pressure data of CH_4, CO_2, N_2, and SF_6 adsorption isotherms recorded at 293 K of V-TBAPy.

Gas	Intercept (mmol g^{-1})	Slope (mmol g^{-1} kPa^{-1})	R^2	Ideal SF_6/N_2 selectivity	Ideal CO_2/N_2 selectivity
SF_6	0.00442	0.18169	0.99977	53.75	15.83
CO_2	0.00453	0.05352	0.99982		
CH_4	0.00005	0.01053	1		
N_2	0.00001	0.00338	1		

Table S13. Linear fitting parameters and calculated ideal SF_6/N_2, CO_2/N_2 selectivities from low-pressure data of CH_4, CO_2, N_2, and SF_6 adsorption isotherms recorded at 293 K of Ga-TBAPy.

Gas	Intercept (mmol g^{-1})	Slope (mmol g^{-1} kPa^{-1})	R^2	Ideal SF_6/N_2 selectivity	Ideal CO_2/N_2 selectivity
SF_6	0.00534	0.17957	0.99954	47.51	17.02
CO_2	0.00627	0.06433	0.99948		
CH_4	0.00006	0.01126	1		
N_2	0.00002	0.00378	1		

Table S14. Linear fitting parameters and calculated ideal SF_6/N_2, CO_2/N_2 selectivities from low-pressure data of CH_4, CO_2, N_2, and SF_6 adsorption isotherms recorded at 293 K of V-TCPB.

Gas	Intercept (mmol g^{-1})	Slope (mmol g^{-1} kPa^{-1})	R^2	Ideal SF_6/N_2 selectivity	Ideal CO_2/N_2 selectivity
SF_6	0.05441	1.68071	0.98883	365.37	12.77
CO_2	0.00384	0.05873	0.99998		
CH_4	0.00019	0.01912	1		
N_2	0.00002	0.00460	1		

Table S15. Linear fitting parameters and calculated ideal SF_6/N_2, CO_2/N_2 selectivities from low-pressure data of CH_4, CO_2, N_2, and SF_6 adsorption isotherms recorded at 293 K of Ga-TCPB.

Gas	Intercept (mmol g^{-1})	Slope (mmol g^{-1} kPa^{-1})	R^2	Ideal SF_6/N_2 selectivity	Ideal CO_2/N_2 selectivity
SF_6	-0.01938	1.38600	0.99982	437.22	15.66
CO_2	0.00165	0.04963	0.99999		
CH_4	0.00195	0.01475	0.99857		
N_2	0.00146	0.00317	0.98115		

Section S6.2.2. Ideal adsorption solution theory (IAST) selectivity

The pure-component SF_6 and N_2 isotherms recorded at 293 K were modeled using the Langmuir (Eq. 3) or dual-site Langmuir models (Eq. 4):

$$N_{eq} = \frac{N_{1,sat} b_1 P}{1 + b_1 P} \quad [3]$$

$$N_{eq} = \frac{N_{1,sat} b_1 P}{1 + b_1 P} + \frac{N_{2,sat} b_2 P}{1 + b_2 P} \quad [4]$$

Where N_{eq} (mmol g^{-1}) is the quantity of gas adsorbed under equilibrium at pressure P (kPa), $N_{1,sat}$ and $N_{2,sat}$ (mmol g^{-1}) are the maximum adsorption capacities of sites 1 and 2, and b_1 and b_2 (kPa^{-1}) are the Langmuir equilibrium constants.

IAST calculations were furthermore carried out for a theoretical gas mixture containing SF_6/N_2 (10:90) using the fitted isotherms in accordance with the IAST equations presented by Myers and Prausnitz[25].

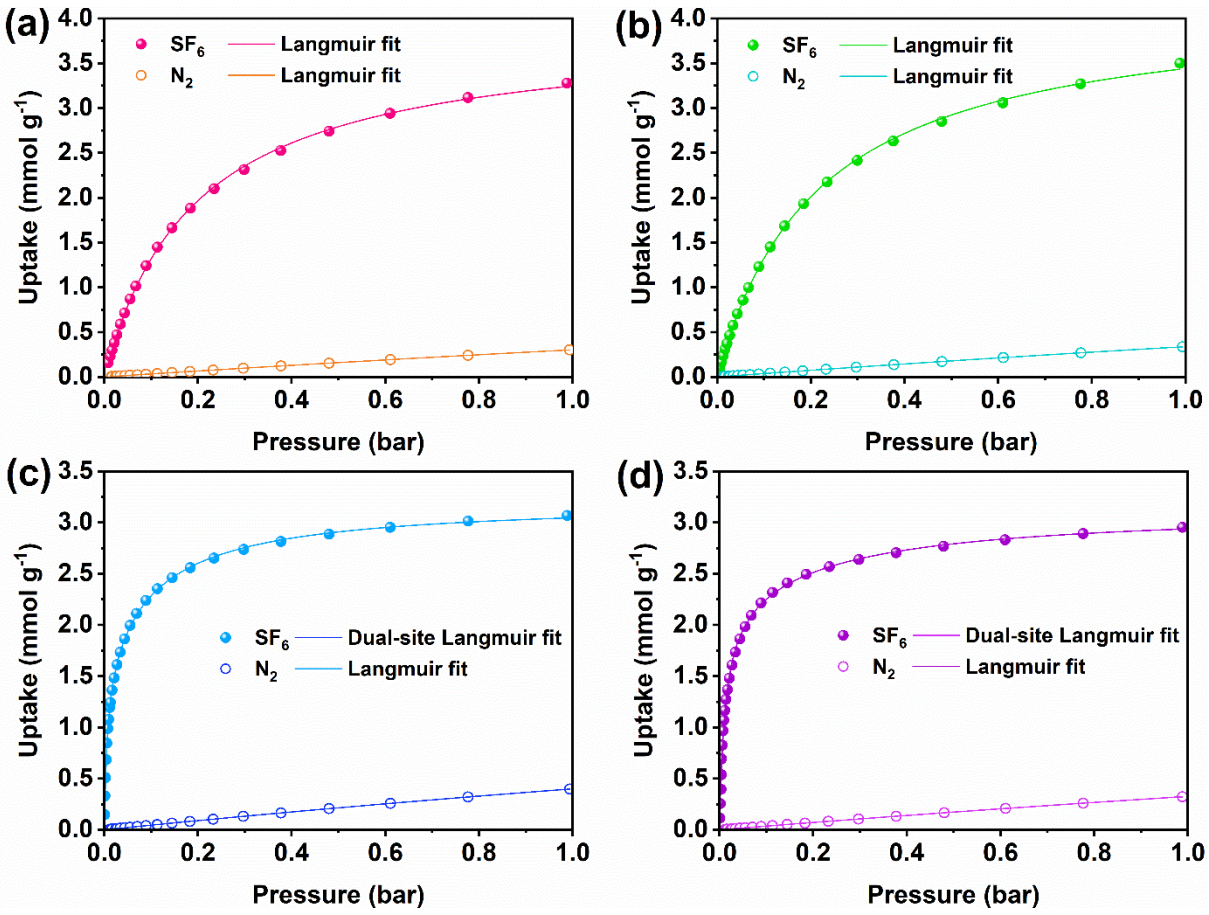

Fig. S31. Langmuir and dual-site Langmuir fits of CO_2 and N_2 adsorption isotherms recorded at 293 K for (a) V-TBAPy, (b) Ga-TBAPy, (c) V-TCPB, and (d) Ga-TCPB.

Table S16. Langmuir and dual-site Langmuir fitting parameters for CO_2 adsorption isotherms recorded at 293 K of V-TBAPy, Ga-TBAPy, V-TCPB, and Ga-TCPB.

	V-TBAPy	**Ga-TBAPy**	**V-TCPB**	**Ga-TCPB**
$N_{1,sat}$ (mmol g^{-1})	3.87684	4.18311	1.58472	2.16207
b_1 (bar^{-1})	5.15984	4.64016	162.92417	91.00422
$N_{2,sat}$ (mmol g^{-1})	-	-	1.62618	0.97692
b_2 (bar^{-1})	-	-	9.49274	4.51466
RMSE	0.01834	0.01953	0.01220	0.03609

Table S17. Langmuir fitting parameters for N_2 adsorption isotherms recorded at 293 K of V-TBAPy, Ga-TBAPy, V-TCPB, and Ga-TCPB.

	V-TBAPy	**Ga-TBAPy**	**V-TCPB**	**Ga-TCPB**
$N_{1,sat}$ (mmol g^{-1})	2.86370	3.12058	2.95920	2.92551
b_1 (bar^{-1})	0.11813	0.12150	0.15631	0.12558
RMSE	0.00012	0.00010	0.00002	0.00001

Section S7. SF_6 and CO_2 temperature-swing adsorption cycling

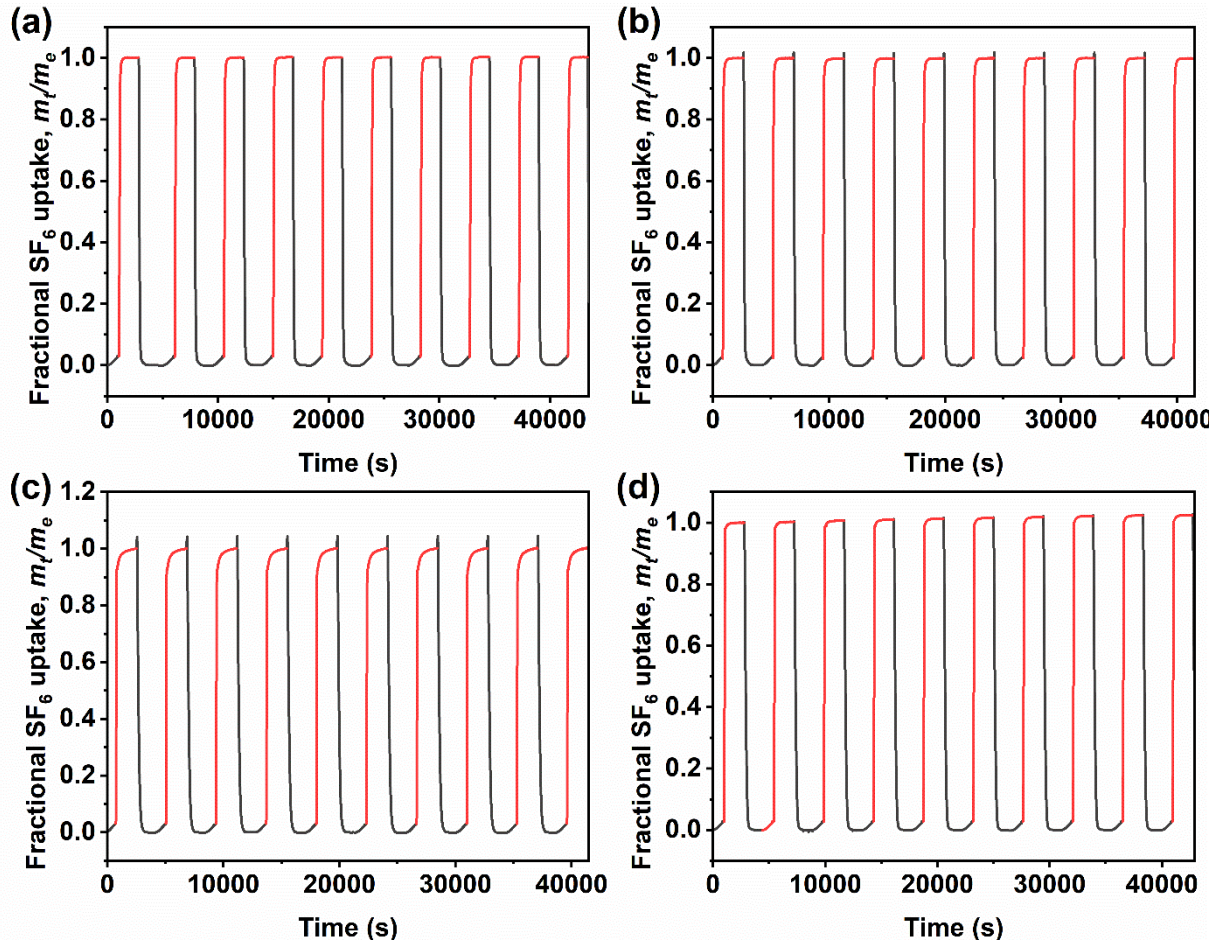

Fig. S32. Gravimetric temperature-swing adsorption cycling of SF_6 on (a) V-TBAPy, (b) Ga-TBAPy, and (c) Ga-TBAPy. The adsorption and desorption part of the cycles are highlighted in red and black, respectively.

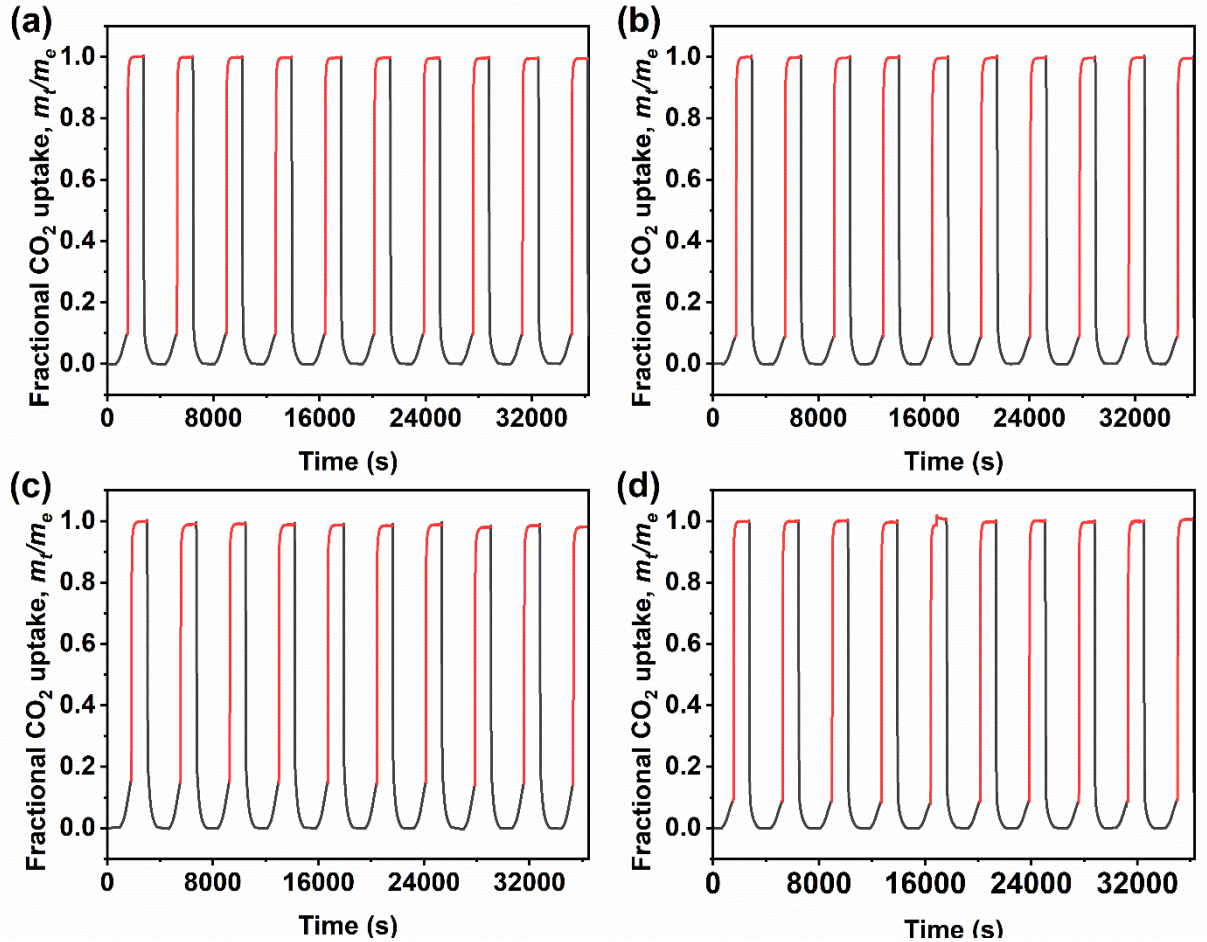

Fig. S33. Gravimetric temperature-swing adsorption cycling of CO_2 on (a) V-TABPy, (b) Ga-TBAPy, (c) V-TCPB, and (d) Ga-TCPB. The adsorption and desorption part of the cycles are highlighted in red and black, respectively.

References

1. P. Oleynikov, 2011.
2. W. Kabsch, *Acta Crystallogr. D Biol. Crystallogr.*, 2010, **66**, 125-132.
3. O. V. Dolomanov, L. J. Bourhis, R. J. Gildea, J. A. K. Howard and H. Puschmann, *J. Appl. Crystallogr.*, 2009, **42**, 339-341.
4. G. M. Sheldrick, *Acta Crystallogr. A Found. Adv.*, 2015, **71**, 3-8.
5. G. M. Sheldrick, *Acta Crystallogr. C Struct. Chem.*, 2015, **71**, 3-8.
6. G. L. Marra, A. N. Fitch, A. Zecchina, G. Ricchiardi, M. Salvalaggio, S. Bordiga and C. Lamberti, *J. Phys. Chem. B*, 1997, **101**, 10653–10660.
7. H. M. Rietveld, *Aust. J. Phys.*, 1988, **41**, 113-116.
8. V. Petříček, M. Dušek and L. Palatinus, *Z. Kristallogr. Cryst. Mater.*, 2014, **229**, 345-352.
9. K. Momma and F. Izumi, *J. Appl. Crystallogr.*, 2011, **44**, 1272-1276.
10. Y.-Y. Liu, S. Couck, M. Vandichel, M. Grzywa, K. Leus, S. Biswas, D. Volkmer, J. Gascon, F. Kapteijn, J. F. M. Denayer, M. Waroquier, V. Van Speybroeck and P. Van Der Voort, *Inorg. Chem.*, 2013, **52**, 113-120.
11. G. Silversmit, D. Depla, H. Poelman, G. B. Marin and R. De Gryse, *J. Electron Spectrosc. Relat. Phenom.*, 2004, **135**, 167-175.

12. J. Ren, M. Chang, W. Zeng, Y. Xia, D. Liu, G. Maurin and Q. Yang, *Chem. Mater.*, 2021, **33**, 5108-5114.
13. L. Yan, H.-T. Zheng, L. Song, Z.-W. Wei, J.-J. Jiang and C.-Y. Su, *Chem. Eng. J.*, 2023, **472**.
14. S.-M. Wang, X.-T. Mu, H.-R. Liu, S.-T. Zheng and Q.-Y. Yang, *Angew. Chem. Int. Ed.*, 2022, **61**, e202207066.
15. M. Chang, T. Yan, Y. Wei, J.-X. Wang, D. Liu and J.-F. Chen, *Chem. Mater.*, 2022, **34**, 9134-9143.
16. M.-B. Kim, S.-J. Lee, C. Y. Lee and Y.-S. Bae, *Microporous Mesoporous Mater.*, 2014, **190**, 356-361.
17. S.-T. Zheng, R.-Y. Jiang, Y. Jiang, S. Ni, G.-W. Guan, S.-Q. Shao, Y.-C. Wang, S.-M. Wang and Q.-Y. Yang, *Sep. Purif. Technol.*, 2023, **318**.
18. P. Liu, T. Zhao, K. Cai, P. Chen, F. Liu and D.-J. Tao, *Chem. Eng. J.*, 2022, **437**.
19. Y. Hu, L. Wang, R. Nan, N. Xu, Y. Jiang, D. Wang, T. Yan, D. Liu, Y. Zhang and B. Chen, *Chem. Eng. J.*, 2023, **471**.
20. T. Wang, M. Chang, T. Yan, Y. Ying, Q. Yang and D. Liu, *Ind. Eng. Chem. Res.*, 2021, **60**, 5976-5983.
21. M.-B. Kim, K.-M. Kim, T.-H. Kim, T.-U. Yoon, E.-J. Kim, J.-H. Kim and Y.-S. Bae, *Chem. Eng. J.*, 2018, **339**, 223-229.
22. M.-B. Kim, T.-H. Kim, T.-U. Yoon, J. H. Kang, J.-H. Kim and Y.-S. Bae, *JIEC*, 2020, **84**, 179-184.
23. M.-B. Kim, T.-U. Yoon, D.-Y. Hong, S.-Y. Kim, S.-J. Lee, S.-I. Kim, S.-K. Lee, J.-S. Chang and Y.-S. Bae, *Chem. Eng. J.*, 2015, **276**, 315-321.
24. L. Czepirski and J. JagiełŁo, *Chem. Eng. Sci.*, 1989, **44**, 797-801.
25. A. L. Myers and J. M. Prausnitz, *AlChE J.*, 1965, **11**, 121-127.